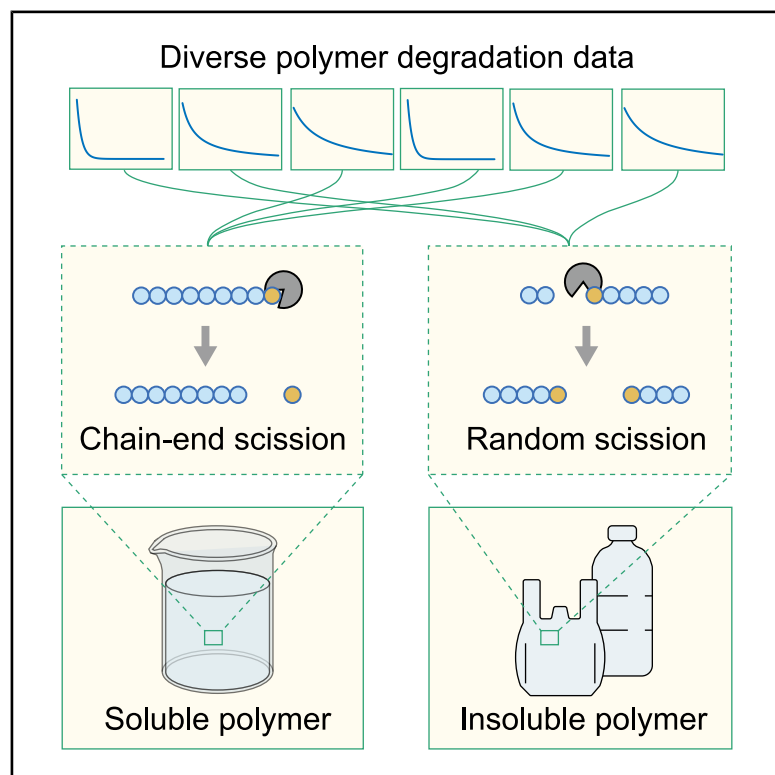


# Revealing chain scission modes in variable polymer degradation kinetics

## Graphical abstract



## Authors

Yijie Cheng, Adolfo Lopez,  
Tsz Hung Wong, Darryl Francis,  
Emily England, Xinyue Liu

## Correspondence

xylu@msu.edu

## In brief

Polymer degradation pathways, whether their bonds break at the chain ends or randomly along the backbone, have long been considered stochastic. Cheng et al. integrate data mining with mechanistic modeling across various polymer systems to reveal that solubility, not molecular structure alone, dictates the dominant chain scission mode. Soluble polymers degrade via chain-end scission, and insoluble polymers degrade randomly. These findings establish a new framework for predicting degradation behavior, enabling smarter design of environmentally responsive and sustainable polymer materials.

## Highlights

- Uncover polymer degradation rules across diverse and varied polymers
- Decode polymer chain scission modes from accessible molecular weight decay data
- Leverage mechanistic modeling to reveal degradation pathways beyond empirical fits
- Identify polymer solubility as the key factor differentiating polymer scission modes



## Article

# Revealing chain scission modes in variable polymer degradation kinetics

Yijie Cheng,<sup>1</sup> Adolfo Lopez,<sup>2</sup> Tsz Hung Wong,<sup>2</sup> Darryl Francis,<sup>1</sup> Emily England,<sup>1</sup> and Xinyue Liu<sup>1,3,\*</sup>

<sup>1</sup>Department of Chemical Engineering and Materials Science, Michigan State University, East Lansing, MI 48824, USA

<sup>2</sup>Department of Mechanical Engineering, Michigan State University, East Lansing, MI 48824, USA

<sup>3</sup>Lead contact

\*Correspondence: [xyliu@msu.edu](mailto:xyliu@msu.edu)

<https://doi.org/10.1016/j.newton.2025.100168>

**ACCESSIBLE OVERVIEW** Imagine a pearl necklace: if you cut the string at one end, the pearls fall off one by one, but if you cut it in the middle, the necklace splits into two parts. Polymer chains degrade in similar ways, either sequentially from the chain ends (chain-end scission) or randomly along the backbone (random scission). But unlike cutting a necklace, polymer degradation is not purely a chance event, and it is dictated by both structural factors and the surrounding environment of the material. This study analyzes time-dependent molecular weight data from a variety of polymers degraded under diverse experimental conditions. By fitting the data to two established degradation models, it is identified whether a polymer primarily undergoes chain-end or random scission. Statistical analysis reveals that solubility is the most important factor, as soluble polymers tend to degrade from the ends, and insoluble polymers, such as plastics in aqueous environments, tend to break randomly throughout the chain. In contrast, factors such as molecular weight, degradable bonds, and crystallinity showed little correlation with the polymer degradation mode. These results overturn the common assumption that polymer degradation is governed primarily by molecular chemistry alone. Instead, the study shows that the polymer's physical state, specifically its ability to dissolve, strongly influences how it breaks down at the molecular level. This insight offers a predictive framework for designing polymers with targeted degradation pathways with numerous applications, from biodegradable packaging and agricultural films to drug delivery vehicles and temporary tissue scaffolds.

## SUMMARY

Polymer degradation depends on environmental conditions and molecular structures. While existing studies provide individual degradation kinetics for specific chemistries and environments, a comprehensive analysis across diverse datasets is necessary to uncover universal degradation principles across different polymers. In this study, we conduct a meta-analysis integrating data mining and mechanistic modeling. We first collect various time-dependent molecular weight datasets and evaluate how well two models (chain-end scission and random scission) fit each dataset, which allows us to identify the dominant chain scission mode for each case. Our correlation analysis shows that, among all structural factors, polymer solubility plays a critical role. Soluble polymers tend to degrade from the chain ends, while insoluble polymers break more randomly along the backbone. These findings provide cross-scale insights into the molecular mechanisms that dictate polymer degradation and offer new guidelines for the design of sustainable polymers with controlled and predictable degradation behavior toward environmental and biomedical applications.

## INTRODUCTION

Sustainable polymers play a vital role in addressing the environmental challenges posed by traditional plastics, as these materials are designed to degrade under specific conditions.<sup>1,2</sup> Degradation of these sustainable polymers is a complex process involving simultaneous molecular reactions and mass transport, which are also influenced by diverse environmental factors.<sup>3–6</sup>

Understanding this multiphysics and multifactorial material behavior requires a comprehensive analytical approach beyond isolated experimental observations. While recent studies have reported individual degradation data points, these are primarily based on specific molecular chemistries and bulk structures,<sup>7–10</sup> hindering the discovery of universal degradation principles that rely on the full spectrum of datasets. One fundamental aspect associated with macroscopic polymer degradation is the chain



scission modes at the molecular scale.<sup>4,11</sup> The chain scission mode, either chain-end depolymerization or random scission,<sup>12–15</sup> is crucial in dictating degradation kinetics, thereby impacting the design of polymers with programmable degradation profiles and the optimization of catalytic conditions. However, understanding the chain scission mode from individual degradation kinetics measurements remains unclear.

Polymer informatics has emerged as a promising meta-analysis approach that leverages large-scale data mined from the literature to uncover universal principles in polymer degradation,<sup>16,17</sup> which enables accurate property predictions and knowledge generation. However, current efforts in polymer informatics have primarily focused on data-driven statistical analysis without incorporating mechanistic modeling,<sup>18,19</sup> which limits the ability to reveal fundamental insights. In fact, polymer degradation is governed by well-defined chemical reactions,<sup>20</sup> chain scission pathways,<sup>4</sup> and mass transport phenomena<sup>4,5</sup> rather than being purely stochastic. When applying informatics to polymer degradation, two additional technical challenges remain to be addressed: first, most polymer databases represent degradation behavior using a single numerical value, such as a degradation rate,<sup>17,21</sup> which fails to capture the time-evolving degradation process and uncover chain scission mechanisms. Second, the degradation data are highly condition-dependent, with variations in sample size,<sup>22</sup> morphology,<sup>5</sup> solvent environment,<sup>23,24</sup> and measurement techniques significantly influencing reported outcomes, which further complicates cross-study comparisons.<sup>5</sup> Overcoming these barriers requires a systematic informatics strategy that extracts full kinetic information for comprehensive data collection, integrates mechanistic modeling for enhanced data interpretation, and establishes standardized degradation parameters for reliable data analysis, revealing meaningful insights from a wide range of reported polymer degradation data.

Here, our strategy integrates data mining with mechanistic model-based analysis to establish correlations between chain scission modes and key polymer characteristics. Our dataset, compiled through systematic reviews, includes time-dependent molecular weight (MW) measurements from 41 different degrading polymers under various experimental conditions. The raw degradation data were subsequently fitted to two mechanistic models that included chain-end scission and random scission, respectively, and the goodness of fit was assessed using the coefficient of determination ( $R^2$ ). The ratio of  $R^2$  values for both models served as a criterion to classify the dominant chain scission mode for each polymer. To identify key structural factors influencing scission mechanisms, we performed a Pearson correlation analysis on variables such as initial MW, fraction of degradable bonds, polymer solubility, polymer crystallinity, catalyst size, and reaction rate constants. The analysis revealed that chain-end scission is prevalent in soluble polymers and that random scission dominates at the solid-liquid interface in bulk plastics (Pearson's correlation coefficient,  $\rho = 0.67$ ). Meanwhile, other chemical structural factors (e.g., initial MW, degradable bond fraction, catalyst size, and polymer crystallinity) showed no significant correlation with the chain scission mode ( $|\rho| < 0.05$ ). These findings provide new insights into the molecular mechanisms governing polymer degradation and facilitate

the rational design of sustainable materials with programmable degradation profiles.

## RESULTS

### Polymer degradation data extraction via systematic review

This study focuses on the hydrolytic and enzymatic degradation of polymers, which are the predominant pathways for sustainable polymer breakdown.<sup>5,25</sup> Microscopically, the catalytic species (e.g., water, acid, base, ions, radicals, or enzymes) break down the labile bonds (e.g., ester bond,<sup>26–28</sup>  $\beta$ -1,4-glycosidic bond,<sup>29</sup> carbonate bond,<sup>30</sup> phosphazene bond,<sup>31</sup> or anhydride bond<sup>32</sup>). Macroscopically, these degradable polymers undergo distinct erosion processes depending on the polymer's physical form.<sup>33</sup> Soluble polymers degrade through bulk erosion, where the degradation reaction occurs at the single-chain level uniformly throughout the material.<sup>34</sup> On the other hand, insoluble polymers undergo surface erosion, where the degradation reaction is limited to the interface between the solid and the surrounding medium.<sup>35</sup> To experimentally characterize polymer degradation kinetics, researchers have employed various metrics, including the degradation timescale (or rate constant), mass loss over time,<sup>36</sup> MW reduction,<sup>7</sup> and mechanical property decay.<sup>37</sup> Among these, tracking the MW over time has been widely adopted as a robust metric of polymer degradation kinetics because it provides transient information about the fundamental chain scission events. For soluble polymers, MW distributions (MWDs) are measured at different time points using gel permeation chromatography (GPC), size-exclusion chromatography (SEC), mass spectrometry (MS), or viscometry.<sup>38,39</sup> For insoluble polymers, the whole material, including degraded fragments and undegraded pieces, is first dissolved in an appropriate solvent, followed by determining the MWDs using the same techniques (Figure 1A).<sup>40</sup>

To systematically extract time-dependent MW data from existing research, we conducted a comprehensive systematic review of published polymer degradation studies since 2000 using Google Scholar, including a total of 16,400 papers on hydrolytic and enzymatic degradation. Among these, 28 studies were identified that reported MW kinetics across diverse polymer types and experimental conditions. Unlike single-point measurements, the dataset of time-dependent MW captures full degradation kinetics, providing time-dependent MW curves across a broad spectrum of degradation conditions, polymer chemistries, and material forms. The compiled dataset includes 41 MW decay curves and 411 MW measurements in total, representing polymers of varying chemical compositions (including natural, water-soluble polymers such as chitosan,<sup>41</sup> alginate,<sup>45</sup> and citrus pectin,<sup>43</sup> as well as synthetic polymers such as poly(lactic acid) [PLA],<sup>50</sup> polycaprolactone [PCL],<sup>23,51</sup> and polyphosphazene<sup>42</sup>), catalytic degradation pathways (including hydrolytic,<sup>50</sup> metal ion-mediated,<sup>7</sup> peroxide-catalyzed,<sup>41,45</sup> enzyme-assisted,<sup>29</sup> and microbial<sup>52</sup> degradation), physical forms (either solid plastics or polymer solution), initial MWs (from 4 to 2,000 kDa), and degradation time frames (from 1 h to 3.3 years). For the MW data, we specifically select the number-average MW rather than the weight-average or z-average MW, intrinsic viscosity, and others to ensure consistency with

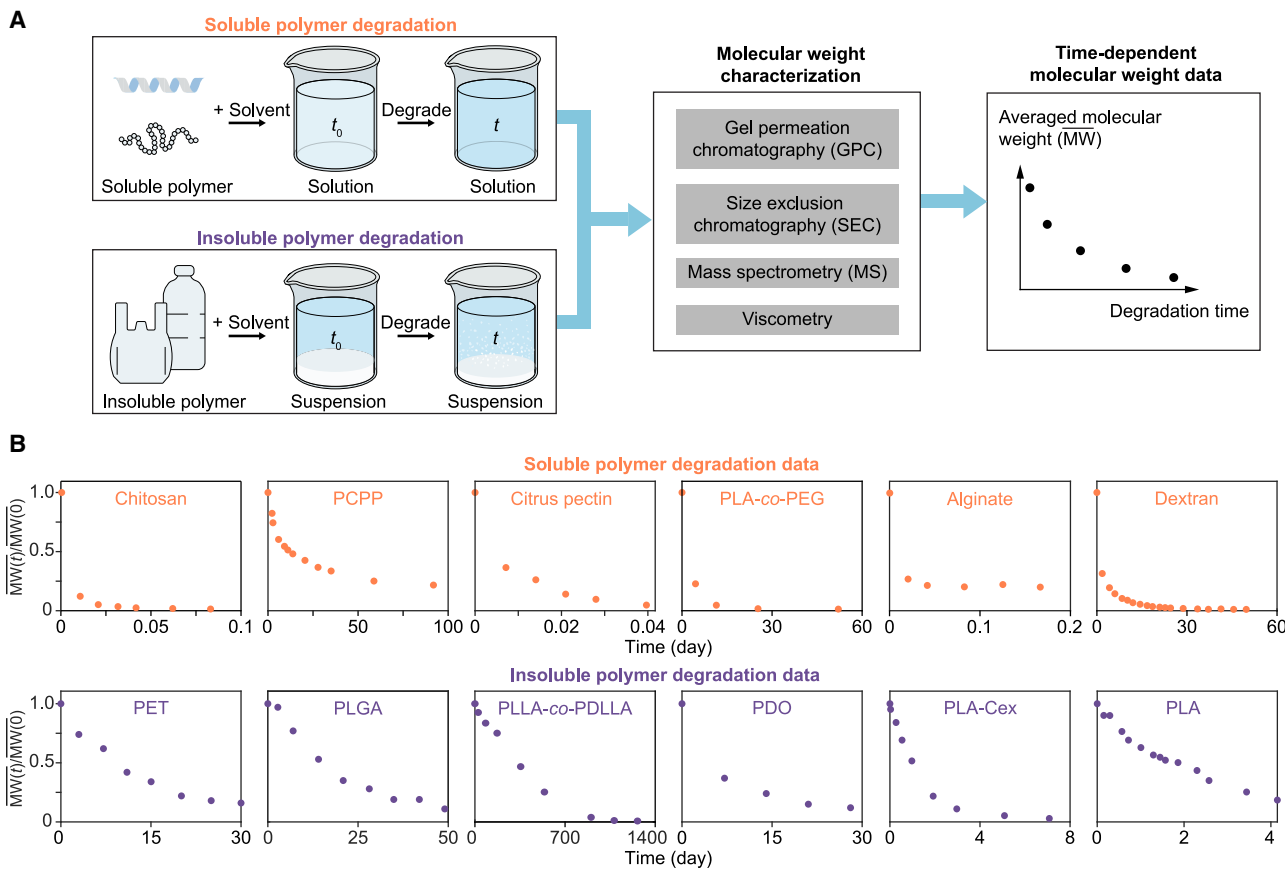


**Figure 1. Data extraction of polymer degradation based on molecular weight reduction**

(A) Schematics of soluble and insoluble polymer degradation, where soluble polymers dissolve in the solvent before degradation, whereas insoluble polymers form suspensions. The molecular weight (MW) of the polymers is characterized over time, providing time-dependent MW decay curves.

(B) Time-dependent MW degradation data for selected polymers by plotting  $\bar{M}_W(t)/\bar{M}_W(0)$  as a function of time for different polymer types. Soluble polymers (top row, orange) include chitosan,<sup>41</sup> poly[di(carboxylatophenoxy)phosphazene] (PCPP),<sup>42</sup> citrus pectin,<sup>43</sup> polylactide-co-poly(ethylene glycol) (PLA-co-PEG),<sup>44</sup> alginate,<sup>45</sup> and dextran,<sup>29</sup> and insoluble polymers (bottom row, purple) include poly(ethylene terephthalate) (PET),<sup>46</sup> poly(lactic-co-glycolic acid) (PLGA),<sup>47</sup> poly(D,L-lactide)-co-poly(D,L-lactide) (PLLA-co-PDLA),<sup>48</sup> polydioxanone (PDO),<sup>40</sup> poly(lactic acid) with chain extender (PLA-Cex),<sup>49</sup> and poly(lactic acid) (PLA).<sup>50</sup>

the mathematical models. In addition, the number-average MW provides a direct measure of the average polymer chain length, making it particularly suitable for analyzing chain scission mechanisms.

To compare degradation trends, we selected representative data for six soluble and six insoluble polymers and plotted the averaged and normalized MW ( $\bar{M}_W(t)/\bar{M}_W(0)$ ) as a function of time (Figure 1B). The full dataset, comprising 41 polymer degradation curves, is provided in Table S1 and Figure S1. While all polymers exhibit MW decay over time (i.e.,  $\bar{M}_W(t)/\bar{M}_W(0)$  from 1 to 0), their degradation kinetics vary significantly in curve shape and timescale due to different polymer structures and degradation mechanisms. Direct statistical comparisons of these data without incorporating physical models remain insufficient to extract meaningful insights. For example, parameters like directly calculated degradation rates can describe the overall degradation performance, but they primarily reflect coupled mass transport and reaction rates rather than revealing the intrinsic chain cleavage mechanisms at the molecular level.

### Mechanistic modeling for chain scission in polymer degradation

To establish a direct correlation between degradation kinetics and molecular-level mechanisms, we employ a theoretical framework of polymer degradation kinetics developed by McCoy and Madras<sup>53,54</sup> that utilizes population balance models to describe the time evolution of MWDs under different chain scission modes. While this theoretical framework has successfully classified chain scission modes in specific polymer degradation cases,<sup>11</sup> much of the existing research only provides averaged data rather than the full distribution of the MW, leaving many degradation mechanisms unexamined.<sup>7,39,40,55–57</sup> Here, we leverage population balance calculations to derive the number-average MW decay at various reaction extents and provide a mechanistic interpretation of degradation kinetics.

Polymer degradation kinetics are inherently linked to changes in chain length or degree of polymerization (DOP) distributions over time. We define  $p(x, t)$  as the molar concentration of the polymer with a DOP of  $x$  at time  $t$  (Note S1) and express the molar concentration as  $c_{\text{mole}}(t) = \int_0^{\infty} p(x, t)dx$  and the mass

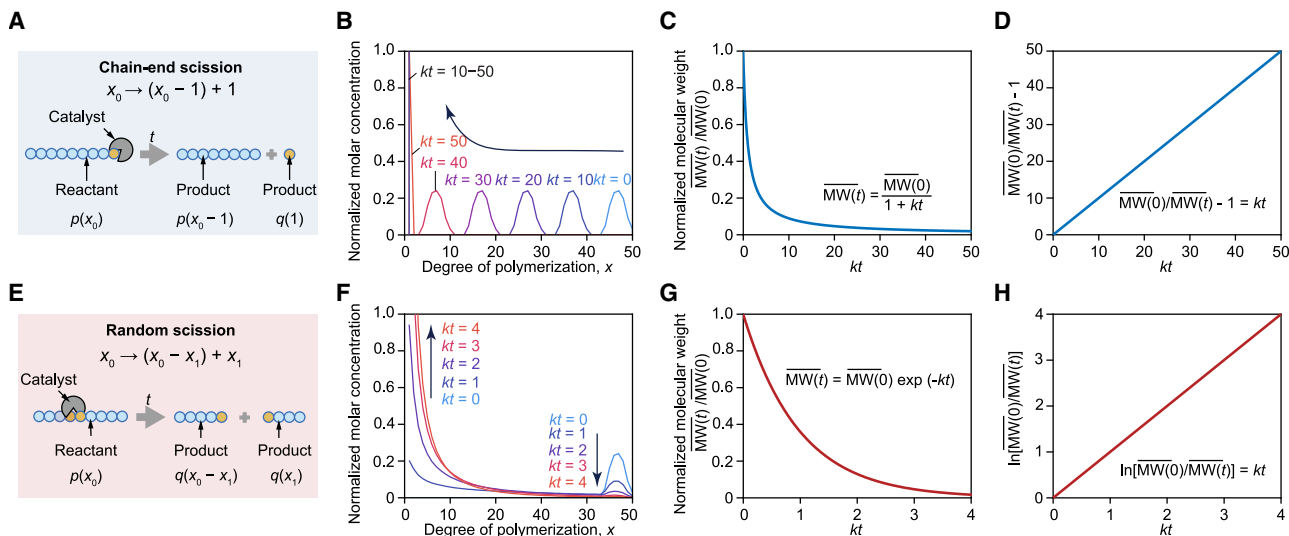


**Figure 2. Mathematical modeling of degradation kinetics for chain-end and random scission modes**

- (A) Schematics of a chain-end scission reaction in which a polymer molecule with the chain length  $x_0$  fragments into another polymer molecule of  $(x_0 - 1)$  and a monomer molecule.
- (B) Evolution of molar concentration distributions over time when the polymer undergoes chain-end scission, showing a shift toward low MW as degradation progresses ( $kt = 0-50$ ).
- (C) Evolution of the normalized molecular weight  $MW(t)/\overline{MW(0)}$  decay over time for chain-end scission.
- (D) Evolution of  $(\overline{MW(0)}/\overline{MW(t)} - 1)$  over time for chain-end scission, exhibiting a linear relationship.
- (E) Schematics of a random scission reaction, in which a polymer molecule with the chain length  $x_0$  fragments into two polymer molecules with the chain lengths  $(x_0 - x_1)$  and  $x_1$ .
- (F) Evolution of molar concentration distributions over time when the polymer undergoes random scission, showing an increasing fraction of low-MW species.
- (G) Evolution of the normalized molecular weight  $MW(t)/\overline{MW(0)}$  decay over time for random scission.
- (H) Evolution of  $\ln(\overline{MW(0)}/\overline{MW(t)})$  over time for random scission, exhibiting a linear relationship.

concentration as  $c_{\text{mass}}(t) = \int_0^\infty p(x, t) dx$ . The number-average MW at time  $t$  is given by  $\overline{MW(t)} = c_{\text{mass}}(t)/c_{\text{mole}}(t)$ . The evolution of DOP distribution  $p(x, t)$  depends on the specific chain scission mechanism: chain-end scission (which cleaves bonds exclusively at the polymer terminal) or random scission (where bonds break at any position along the backbone with equal probability).

In chain-end scission, since degradation proceeds through sequential cleavage of monomer units from polymer chain terminals, the degradation reaction follows



where  $x_0$  is the DOP of the initial reactant polymer prior to any chain cleavage events and  $(x_0 - 1)$  and 1 are the DOPs of degraded products (Figure 2A). The population balance equation governing this process is

$$dp(x, t)/dt = -kp(x, t) + kp(x + 1, t), \quad (\text{Equation 2})$$

where  $k$  is the rate constant for the chain-end cleavage and  $x$  denotes the DOP of intermediate polymers, which acts as both the reactant and product ( $x > 1$ ). For the monomer product, the rate expression from the population balance is

$$dq(1, t)/dt = k \int_0^\infty p(x, t) dx. \quad (\text{Equation 3})$$

By numerically solving the population balance equations with initial conditions  $p(x, 0)$ , we obtain the full DOP distribution  $p(x, t)$  evolving with reaction extent  $kt$  when polymers undergo chain-end scission (Figure 2B). Using moment analysis (detailed in Note S2 and Figure S2), the time-dependent expressions for molar and mass concentrations are

$$c_{\text{mole}}(t) = c_{\text{mole}}(0)(1 + kt) \quad (\text{Equation 4})$$

and

$$c_{\text{mass}}(t) = c_{\text{mass}}(0), \quad (\text{Equation 5})$$

which leads to the analytic expression of the number-averaged MW

$$\overline{MW(t)} = \overline{MW(0)}/(1 + kt). \quad (\text{Equation 6})$$

When plotting MW decay as a function of  $kt$ , we observe a rapid decrease in MW at the early degradation stage ( $kt < 5$ ) (Figure 2C). A distinguishing feature of chain-end scission is that plotting  $(\overline{MW(0)}/\overline{MW(t)} - 1)$  against time yields a linear increase, providing a diagnostic signature (Figure 2D).

Random chain scission involves breaks at any bond along the polymer backbone with equal possibilities. The reaction sequence in random scission follows



leading to the formation of a mixture of shorter polymers with DOPs of  $(x_0 - x_1)$  and  $x_1$  (Figure 2E). The corresponding population balance equation is

$$\frac{dq(x, t)}{dt} = -kq(x, t) + 2k \int_x^\infty \frac{q(x_i, t)}{x_i} dx_i. \quad (\text{Equation 8})$$

Numerically solving the differential equation yields the time-dependent DOP distribution  $p(x, t)$  (Figure 2F). From moment analysis (Note S3; Figure S3), the molar and mass concentrations for reactants evolve as

$$c_{\text{mole}}(x_0, t) = c_{\text{mole}}(0)e^{-kt} \quad (\text{Equation 9})$$

and

$$c_{\text{mass}}(x_0, t) = c_{\text{mass}}(0)e^{-kt}, \quad (\text{Equation 10})$$

respectively. For degraded products,

$$c_{\text{mole}}(x, t) = c_{\text{mole}}(0)(e^{kt} - e^{-kt}) \quad (\text{Equation 11})$$

and

$$c_{\text{mass}}(x, t) = c_{\text{mass}}(0)(1 - e^{-kt}). \quad (\text{Equation 12})$$

Thereafter, the analytic expression of the average MW is given by

$$\overline{\text{MW}(t)} = \overline{\text{MW}(0)}e^{-kt}, \quad (\text{Equation 13})$$

indicating that random scission results in an exponential decay of polymer MW (Figure 2G). When plotted as  $\ln(\overline{\text{MW}(0)}/\overline{\text{MW}(t)})$  against time, random scission exhibits a linear trend, which distinguishes it from chain-end degradation (Figure 2H).

While the kinetic models adopted in this study provide computational simplicity and analytic solutions, they rely on several assumptions, such as continuously variable chain length, simple reaction schemes, and constant reaction rate coefficients.<sup>58–60</sup> For more complex polymer degradation scenarios, emerging species-tracking techniques, such as finite element methods or kinetic Monte Carlo simulations, are required to capture discrete scission events with higher accuracy.<sup>14,61,62</sup>

### Identification of chain scission modes using reported degradation data

The analytical solutions derived for chain-end and random scission models provide a quantitative framework to distinguish degradation mechanisms based on experimental polymer degradation data. To systematically analyze degradation behavior, the compiled data for all 41 polymers with different polymer types and degradation conditions were plotted using normalized MW decay over time. Each dataset was fitted using both chain-end and random scission models, incorporating both direct MW decay trends (i.e.,  $\overline{\text{MW}(t)}/\overline{\text{MW}(0)}$  vs. time) and their respective linearized transformations (i.e.,  $\overline{\text{MW}(0)}/\overline{\text{MW}(t)} - 1$  vs. time and  $\ln(\overline{\text{MW}(0)}/\overline{\text{MW}(t)})$  vs. time). To classify the dominant chain scission mode for each polymer, we computed the  $R^2$  for both models using their linearized plots. The  $R^2$  values quantify the goodness of fit, and the ratio of  $R^2$  values between the two models was used as a criterion for assigning the most probable chain scission mecha-

nism. For the three soluble polymers (e.g., chitosan,<sup>41</sup> dextran,<sup>29</sup> and polylactide-co-poly(ethylene glycol) [PLA-co-PEG]<sup>44</sup>),  $R^2$  values are higher in the chain-end fit, indicating that these soluble polymers exhibit strong agreement with monomer-by-monomer degradation at the chain end (blue lines in Figures 3A–3C). In contrast, the degradation behavior of three insoluble polymers (e.g., polyethylene terephthalate [PET],<sup>46</sup> PLA,<sup>50</sup> poly (lactic-co-glycolic acid) [PLGA]<sup>47</sup>) aligns more closely with random scission, as evidenced by the exponential MW decay trend and the stronger fit in the  $\ln(\overline{\text{MW}(0)}/\overline{\text{MW}(t)})$  vs. time plot (red lines in Figures 3D–3F). All model fitting results for other polymer degradation data are provided in Figure S1. These results suggest that polymer solubility plays an important role in determining the dominant degradation mechanism, with soluble polymers favoring chain-end scission, while insoluble polymers degrade via random scission.

### Meta-analysis of polymer characteristics in determining chain scission modes

To classify polymer degradation mechanisms among all compiled data, we compared the goodness of fit ( $R^2$  values) for experimentally measured MW decay against both chain-end and random scission models (Figure 4A). Polymers were categorized based on the relative  $R^2$  values, where 19 out of 41 polymers exhibited  $R^2(\text{random}) > R^2(\text{end})$ . For example,  $R^2(\text{random})$  for PLLA-co-PDLLA is 0.9833, while its  $R^2(\text{end})$  is 0.7453, indicating a preference for random scission. Conversely, the remaining 22 polymers showed  $R^2(\text{random}) < R^2(\text{end})$ . For example, PLA-co-PEG's  $R^2(\text{random})$  and  $R^2(\text{end})$  are 0.8275 and 0.9546, respectively, classifying them as chain-end scission. When  $R^2(\text{random})$  and  $R^2(\text{end})$  are very close, both random and chain-end pathways may occur simultaneously.<sup>63–65</sup> To establish a standardized classification indicator for a systematic comparison across polymer types, we adopted the ratio of fitting goodness, which was defined as  $R^2(\text{end})/R^2(\text{random})$ , reflecting the dominant degradation behavior under specific conditions.

To elucidate key structural factors influencing chain scission modes, we conducted a Pearson correlation analysis on a range of polymer characteristics of the chemical composition, mass transport, and degradation timescale. In terms of polymer chemical composition, the initial MW ( $\overline{\text{MW}(0)}$ ) exhibited an extremely weak correlation (Pearson correlation coefficient,  $\rho = 0.0008$  in Figure 4B), while the fraction of degradable bonds per repeat unit also showed a near-zero correlation ( $\rho = -0.0111$ ) (Figures 4C and S4). These minimal influences indicate that both polymer chain length and degradable bond fraction do not strongly influence the degradation pathways. For mass transport effects, the catalyst size and polymer crystallization demonstrated similarly weak correlations ( $\rho = -0.0231$  for catalyst size in Figure 4D and 0.0382 for crystallinity in Figure S5), suggesting that neither catalyst size nor polymer crystallinity strongly dictate the chain scission mode. However, the polymer solubility exhibited a strong correlation with the chain scission mode ( $\rho = 0.6773$ ) (Figure 4E). This observation is consistent with the classification results in Figures 3 and 4A, confirming that soluble polymers predominantly undergo chain-end scission, whereas insoluble polymers favor random scission. Meanwhile, the degradation timescale (1/k) showed a moderate negative correlation ( $\rho = -0.5333$ ) (Figure 4F). For example, insoluble

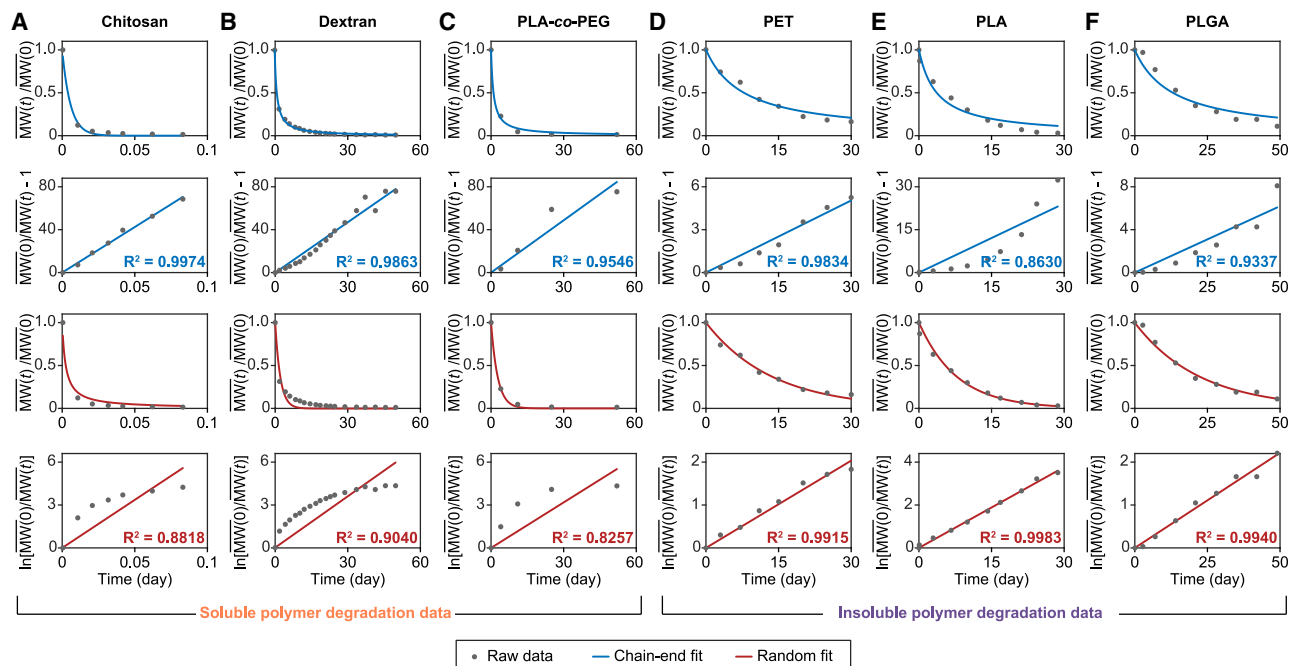


**Figure 3. Fitting polymer degradation data to chain scission mode**

The experimental data of MW decay over time for chitosan (A),<sup>41</sup> dextran (B),<sup>29</sup> PLA-co-PEG (C),<sup>44</sup> PET (D),<sup>46</sup> PLA (E),<sup>50</sup> and PLGA (F)<sup>47</sup> are fitted to chain-end scission (blue line) and random scission (red line) models. The first and second rows show MW decay plots ( $MW(t)/MW(0)$  vs. time) and linearized plots ( $(MW(0)/MW(t) - 1)$  vs. time) for the chain-end scission fitting, with corresponding  $R^2$  values indicating the goodness of fit into the chain-end model. The third and fourth rows show MW decay plots ( $MW(t)/MW(0)$  vs. time) and linearized plots ( $\ln(MW(0)/MW(t))$  vs. time) for the random scission fitting, with corresponding  $R^2$  values indicating the goodness of fit into the random model.

polymers, which predominantly undergo random chain scission, tend to exhibit slower degradation rates or longer timescales (e.g., 100–400 days), while soluble polymer degradation with a chain-end scission mechanism can take only 0.01 days. However, we recognize that this correlation is largely driven by polymer solubility rather than the scission mechanism itself.

The influence of polymer solubility on chain scission modes can be particularly supported by two case studies. For example, PCL, a hydrophobic polymer, degrades differently depending on the solvent environment.<sup>23,51</sup> When dissolved in an organic solvent mixture of dichloromethane (DCM) and methanol, PCL exhibits strong chain-end scission behavior ( $R^2(\text{end})/R^2(\text{random}) = 1.06$ ). However, in aqueous environments where PCL stays as insoluble plastic pieces, the degradation shifts toward random scission ( $R^2(\text{end})/R^2(\text{random}) = 0.989$ ). As another example, water is a poor solvent for PLA, leading to degradation via random scission for almost all PLA materials ( $R^2(\text{end})/R^2(\text{random}) = 0.86$ ). By introducing hydrophilic PEG segments, PLA-co-PEG becomes water-soluble, which not only changes the degradation mechanism to chain-end scission ( $R^2(\text{end})/R^2(\text{random}) = 1.16$ ) but also accelerates the degradation timescale by 2.9 times. As an additional note, some deviations, such as PLA-Con (85°C) ( $R^2(\text{end})/R^2(\text{random}) = 1.06$ , insoluble but chain end) and HA (cell) ( $R^2(\text{end})/R^2(\text{random}) = 0.93$ , soluble but random), suggest that other environmental factors, such as temperature and enzyme mobility, can override the typical solubility-dictated degradation behaviors.

## DISCUSSION

Our meta-analysis reveals that the molecular mechanisms governing polymer degradation are fundamentally impacted by the polymer's physical state, specifically whether it is soluble or insoluble in the surrounding medium. This macroscale distinction plays an essential role in determining the microscale chain scission mode during catalytic degradation. At the same time, several experimental studies have validated this relationship for individual polymers under specific conditions.<sup>28,66</sup> For example, recent work from DelRe et al. employed mass spectroscopy and nuclear magnetic resonance to confirm that random scission dominates when the enzyme molecules attack only the solid-state PCL surface, whereas the chain-end scission occurs when enzyme molecules are uniformly dispersed within the PCL matrix.<sup>28</sup> Our data-driven polymer informatics approach extends these macro- and microscale observations to a broader range of polymer degradation.

To understand the cross-scale causality, we propose that polymer solubility governs the accessibility of degradable bonds for the catalyst molecules, thereby dictating the dominant mode of chain scission. In soluble polymers, the polymer chains are fully dispersed in solutions that contain catalytic species. The terminal degradable bonds have less steric hindrance and higher accessibility compared to internal backbone bonds, making them more susceptible to catalytic attack (Figure 5A). As a result, degradation proceeds sequentially from the chain

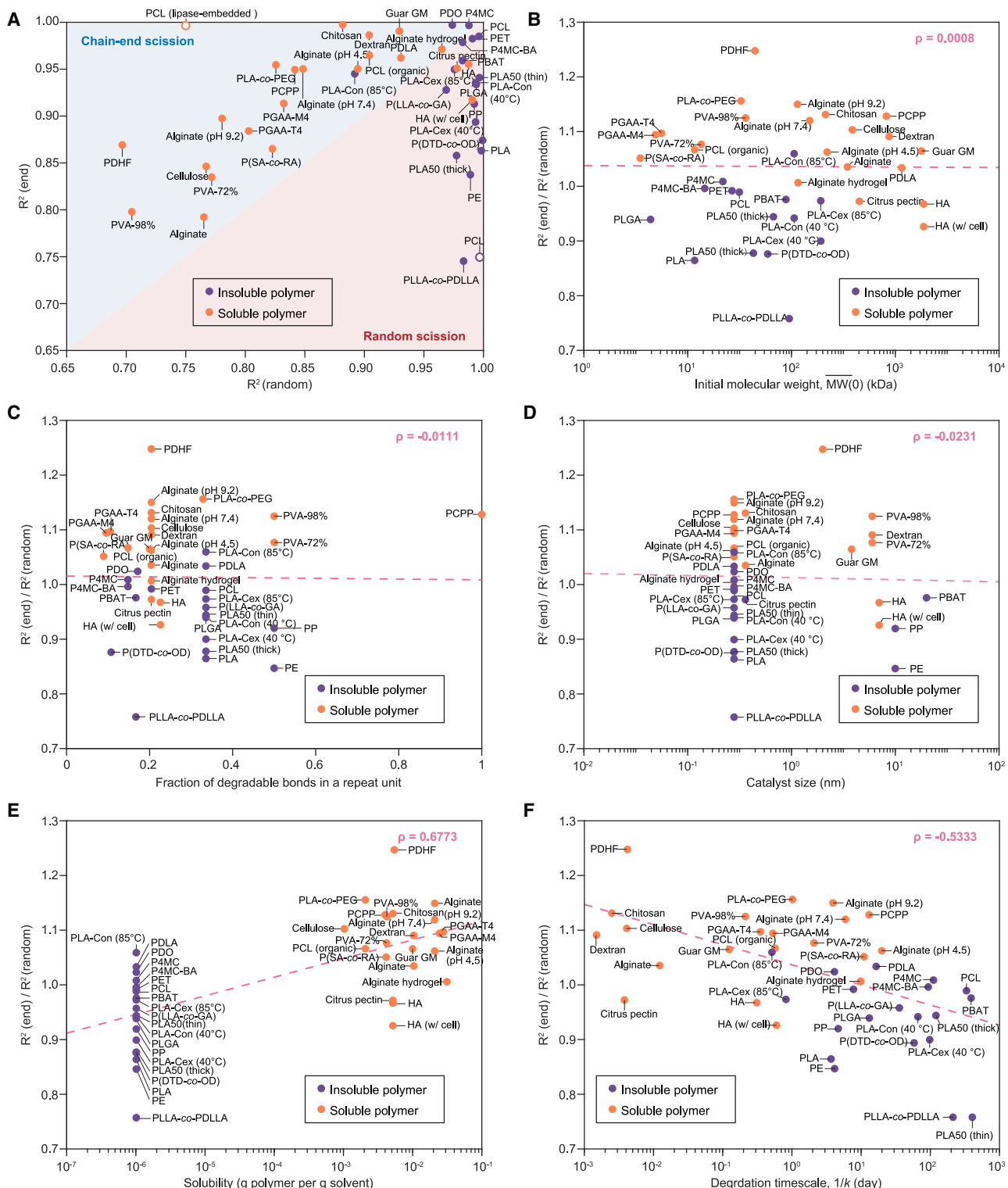


**Figure 4. Pearson correlation analysis of polymer characteristics with chain scission modes**

(A) Classification of polymer chain scission mechanisms based on the coefficient of determination ( $R^2$ ) for chain-end and random scission fitting. Soluble polymers (orange) predominantly follow chain-end scission, while insoluble polymers (purple) align more closely with random scission. Empty circles indicate the polymer degradation with confirmed chain scission modes.<sup>28,66</sup>

(legend continued on next page)

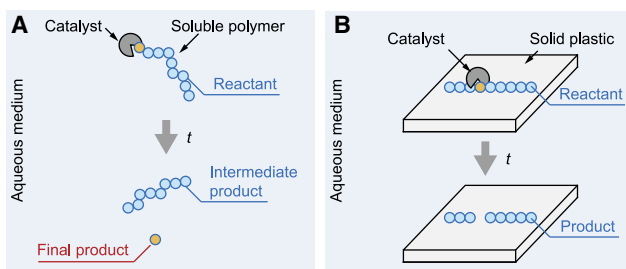


**Figure 5. Hypothetical mechanisms of polymer degradation based on polymer solubility**

(A) Chain-end scission in soluble polymers: due to high accessibility at the polymer chain terminals, degradation occurs sequentially from the end groups, leading to monomer-by-monomer cleavage in dissolved polymer environments.

(B) Random scission in insoluble polymers: in solid plastics, all backbone bonds are equally exposed at the surface, making degradation occur randomly along the polymer chain, resulting in fragmentation rather than sequential depolymerization. The catalysts can be water, acid, base, ions, radicals, or enzymes.

ends, leading to monomer-by-monomer cleavage. In contrast, insoluble polymers remain as solid pieces of plastics, where polymer chains are immobilized rather than dissolved. In this case, all backbone bonds at the solid-liquid interface are equally exposed, and catalysts interact with the polymer surface rather than targeting specific chain ends (Figure 5B). Consequently, bond cleavage occurs randomly along the polymer backbone, leading to random fragmentation rather than sequential depolymerization. This fundamental distinction explains why soluble polymers favor chain-end scission while insoluble polymers predominantly undergo random scission. While our analysis provides quantitative insights into how solubility modulates degradation pathways, high-throughput, real-time, and microscale characterizations are required to validate these mechanistic hypotheses. Such studies would capture transient molecular events across diverse polymer chemistries and verify our proposed causation.

In summary, this study establishes a representative paradigm that combines systematic data mining, theoretical model fitting, and mechanistic meta-analysis to analyze polymer degradation mechanisms, which are often inaccessible through individual experiments. We are able to elucidate polymer chain scission pathways at the molecular level and uncover structure-property relationships for a collection of polymers. These insights will enable the rational design of polymers with programmable degradation profiles and tailororable material performance for applications such as biodegradable plastics, controlled drug release, and sustainable packaging.

Although the current focus is on a physics-informed, data-driven meta-analysis to decode chain scission mechanisms, our framework holds great potential for integration with machine learning (ML) models. By providing structured, physics-consis-

tent datasets as high-quality training inputs for ML algorithms, this approach could enhance ML predictive accuracy for variable polymer chemistries and degradation conditions. Importantly, the inclusion of mechanistic understanding in ML models would bridge the gap between traditional correlation-based learning and physics-informed predictions. Moreover, this high-throughput, physics-informed modeling strategy is extensible to broader polymer informatics applications, enabling the systematic exploration of complex polymer behaviors and the development of novel polymer materials.

## METHODS

Raw polymer degradation data were extracted from the literature using OriginPro 2025 and normalized to the initial MW. The data were subsequently fitted to both chain-end scission and random scission models using MATLAB R2024b. The fitting equations used were as follows:  $\text{MW}(t)/\text{MW}(0) = 1/(1+kt)$  and  $\overline{\text{MW}}(0)/\overline{\text{MW}}(t) - 1 = kt$  for the chain-end scission model and  $\overline{\text{MW}}(t)/\overline{\text{MW}}(0) = e^{-kt}$  and  $\ln[\overline{\text{MW}}(0)/\overline{\text{MW}}(t)] = kt$  for the random scission model. The goodness of fit for each model was evaluated using the  $R^2$ . The ratio of  $R^2$  values between two linear fitting models was used to determine the dominant chain scission mechanism for each polymer. To identify key structural factors influencing scission mechanisms, we performed Pearson correlation analysis using MATLAB R2024b between the  $R^2$  ratio and a series of variables. The Pearson correlation coefficient ( $\rho$ ) was interpreted as follows:  $|\rho| = 0$  indicates no correlation,  $0 < |\rho| \leq 0.2$  indicates a weak correlation,  $0.2 < |\rho| \leq 0.5$  indicates a moderate correlation,  $0.5 < |\rho| \leq 0.8$  indicates a strong correlation, and  $0.8 < |\rho| \leq 1$  indicates a very strong correlation.

## RESOURCE AVAILABILITY

### Lead contact

Further information and requests for resources and reagents should be directed to and will be fulfilled by the lead contact, Xinyue Liu ([xyliu@msu.edu](mailto:xyliu@msu.edu)).

### Materials availability

This study did not generate new unique materials.

### Data and code availability

The raw data and code that support the findings of this study are available at <https://figshare.com/s/a37a03457d1d297c0160>.

## ACKNOWLEDGMENTS

This work was supported in part by the National Science Foundation (CBET-2320716 and CBET-2401017), a Michigan State University faculty start-up grant, and the Tetrad Initiative.

## AUTHOR CONTRIBUTIONS

Conceptualization, Y.C. and X.L.; methodology, Y.C., A.L., T.H.W., D.F., E.E., and X.L.; investigation, Y.C., A.L., and D.F.; theory, Y.C., A.L., and X.L.; writing – original draft, Y.L.; writing – review & editing, Y.C., A.L., T.H.W., D.

(B–F) Correlation analysis of key polymer properties with chain scission preference. The ratio of  $R^2(\text{end})$  to  $R^2(\text{random})$  is plotted against different polymer characteristics, including initial molecular weight (B), fraction of degradable bonds in a repeat unit (C), catalyst size (D), polymer solubility (E), and degradation timescale (F). Pearson correlation coefficients ( $\rho$ ) are indicated for each polymer characteristic.

F., E.E., and X.L.; funding acquisition, X.L.; resources, Y.C. and X.L.; supervision, X.L.

#### DECLARATION OF INTERESTS

The authors declare no competing interests.

#### SUPPLEMENTAL INFORMATION

Supplemental information can be found online at <https://doi.org/10.1016/j.newton.2025.100168>.

Received: March 7, 2025

Revised: May 15, 2025

Accepted: June 13, 2025

Published: July 14, 2025

#### REFERENCES

- Mohanty, A.K., Wu, F., Mincheva, R., Hakkarainen, M., Raquez, J.-M., Mielewski, D.F., Narayan, R., Netravali, A.N., and Misra, M. (2022). Sustainable polymers. *Nat. Rev. Methods Primers* 2, 46.
- Fu, C., Wang, Z., Gao, Y., Zhao, J., Liu, Y., Zhou, X., Qin, R., Pang, Y., Hu, B., Zhang, Y., et al. (2023). Sustainable polymer coating for stainproof fabrics. *Nat. Sustain.* 6, 984–994.
- Abdelfatah, J., Paz, R., Alemán-Domínguez, M.E., Monzón, M., Donate, R., and Winter, G. (2021). Experimental analysis of the enzymatic degradation of polycaprolactone: microcrystalline cellulose composites and numerical method for the prediction of the degraded geometry. *Materials* 14, 2460.
- Pan, Z., and Brassart, L. (2023). A reaction-diffusion framework for hydrolytic degradation of amorphous polymers based on a discrete chain scission model. *Acta Biomater.* 167, 361–373.
- Veskova, J., Sordone, F., and Frisch, H. (2022). Trends in polymer degradation across all scales. *Macromol. Chem. Phys.* 223, 2100472.
- Sanjari, S., Etemadi Haghghi, S., Saraeian, P., and Alinia-ziazi, A. (2024). Modeling Degradation Behavior of (Bio) Degradable Polymers for Medical Devices: A Comparative Review of Physio-chemical Approaches. *J. Polym. Environ.* 33, 660–697.
- Hsu, T.-G., Liu, S., Guan, X., Yoon, S., Zhou, J., Chen, W.-Y., Gaire, S., Seylar, J., Chen, H., Wang, Z., et al. (2023). Mechanochemically accessing a challenging-to-synthesize depolymerizable polymer. *Nat. Commun.* 14, 225.
- Garrison, J.B., Hughes, R.W., and Sumerlin, B.S. (2022). Backbone Degradation of Polymethacrylates via Metal-Free Ambient-Temperature Photo-induced Single-Electron Transfer. *ACS Macro Lett.* 11, 441–446.
- Yang, R., Xu, G., Dong, B., Hou, H., and Wang, Q. (2022). A “polymer to polymer” chemical recycling of PLA plastics by the “DE-RE polymerization” strategy. *Macromolecules* 55, 1726–1735.
- Young, J.B., Hughes, R.W., Tamura, A.M., Bailey, L.S., Stewart, K.A., and Sumerlin, B.S. (2023). Bulk depolymerization of poly (methyl methacrylate) via chain-end initiation for catalyst-free reversion to monomer. *Chem* 9, 2669–2682.
- Tayal, A., and Khan, S.A. (2000). Degradation of a water-soluble polymer: molecular weight changes and chain scission characteristics. *Macromolecules* 33, 9488–9493.
- Hill, A., and Ronan, W. (2022). A kinetic scission model for molecular weight evolution in bioresorbable polymers. *Polym. Eng. Sci.* 62, 3611–3630.
- McCoy, B.J., and Madras, G. (1997). Degradation kinetics of polymers in solution: dynamics of molecular weight distributions. *AIChE J.* 43, 802–810.
- Wang, J., Wang, T.T., Luo, Z.H., and Zhou, Y.N. (2023). Analytical and numerical simulations of depolymerization based on discrete model: A chain-end scission scenario. *AIChE J.* 69, e17854.
- Hoffmann, F., Machatschek, R., and Lendlein, A. (2022). Analytical model and Monte Carlo simulations of polymer degradation with improved chain cut statistics. *J. Mater. Res.* 37, 1093–1101.
- Lin, C., and Zhang, H. (2025). Polymer Biodegradation in Aquatic Environments: A Machine Learning Model Informed by Meta-Analysis of Structure-Biodegradation Relationships. *Environ. Sci. Technol.* 59, 1253–1263.
- McDonald, S.M., Augustine, E.K., Lanners, Q., Rudin, C., Catherine Brinson, L., and Becker, M.L. (2023). Applied machine learning as a driver for polymeric biomaterials design. *Nat. Commun.* 14, 4838.
- Amamoto, Y. (2022). Data-driven approaches for structure-property relationships in polymer science for prediction and understanding. *Polym. J.* 54, 957–967.
- Tao, L., Varshney, V., and Li, Y. (2021). Benchmarking machine learning models for polymer informatics: an example of glass transition temperature. *J. Chem. Inf. Model.* 61, 5395–5413.
- Gewert, B., Plassmann, M.M., and MacLeod, M. (2015). Pathways for degradation of plastic polymers floating in the marine environment. *Environ. Sci. Process. Impacts* 17, 1513–1521.
- Yuan, W., Hibi, Y., Tamura, R., Sumita, M., Nakamura, Y., Naito, M., and Tsuda, K. (2023). Revealing factors influencing polymer degradation with rank-based machine learning. *Patterns* 4, 100846.
- Grizzi, I., Garreau, H., Li, S., and Vert, M. (1995). Hydrolytic degradation of devices based on poly (DL-lactic acid) size-dependence. *Biomaterials* 16, 305–311.
- Hoskins, J.N., and Grayson, S.M. (2009). Synthesis and degradation behavior of cyclic poly ( $\epsilon$ -caprolactone). *Macromolecules* 42, 6406–6413.
- An, W., Liu, X., Li, J., Zhao, X., Long, Y., Xu, S., and Wang, Y.-Z. (2023). Water-solvent regulation on complete hydrolysis of thermosetting polyester and complete separation of degradation products. *J. Hazard. Mater.* 453, 131423.
- Zaaba, N.F., and Jaafar, M. (2020). A review on degradation mechanisms of polylactic acid: Hydrolytic, photodegradative, microbial, and enzymatic degradation. *Polym. Eng. Sci.* 60, 2061–2075.
- Han, X., Liu, W., Huang, J.-W., Ma, J., Zheng, Y., Ko, T.-P., Xu, L., Cheng, Y.-S., Chen, C.-C., and Guo, R.-T. (2017). Structural insight into catalytic mechanism of PET hydrolase. *Nat. Commun.* 8, 2106.
- Chen, C.-C., Dai, L., Ma, L., and Guo, R.-T. (2020). Enzymatic degradation of plant biomass and synthetic polymers. *Nat. Rev. Chem.* 4, 114–126.
- DelRe, C., Jiang, Y., Kang, P., Kwon, J., Hall, A., Jayapurna, I., Ruan, Z., Ma, L., Zolkin, K., Li, T., et al. (2021). Near-complete depolymerization of polyesters with nano-dispersed enzymes. *Nature* 592, 558–563.
- Wang, Q., Liu, T., Xu, X., Chen, H., and Chen, S. (2021). Dextran degradation by sonoenzymolysis: Degradation rate, molecular weight, mass fraction, and degradation kinetics. *Int. J. Biol. Macromol.* 169, 60–66.
- Tsuiji, H. (2022). Hydrolytic degradation. In *Poly (Lactic Acid) Synthesis, Structures, Properties, Processing, Applications, and End of Life*, pp. 467–516.
- Marin, A., Kethanapalli, S.H., and Andrianov, A.K. (2024). Immunopotentiating Polyphosphazene Delivery Systems: Supramolecular Self-Assembly and Stability in the Presence of Plasma Proteins. *Mol. Pharm.* 21, 791–800.
- Reddy, P.G., and Domb, A.J. (2022). Polyanhydride chemistry. *Biomacromolecules* 23, 4959–4984.
- Mndlovu, H., Kumar, P., du Toit, L.C., and Choonara, Y.E. (2024). A review of biomaterial degradation assessment approaches employed in the biomedical field. *npj Mater. Degrad.* 8, 66.
- Li, Y., Wang, S., Qian, S., Liu, Z., Weng, Y., and Zhang, Y. (2024). Depolymerization and Re/Upcycling of Biodegradable PLA Plastics. *ACS Omega* 9, 13509–13521.

35. Tournier, V., Duquesne, S., Guillamot, F., Cramail, H., Taton, D., Marty, A., and André, I. (2023). Enzymes' Power for Plastics Degradation. *Chem. Rev.* **123**, 5612–5701.
36. Kanwal, A., Zhang, M., Sharaf, F., and Li, C. (2022). Enzymatic degradation of poly (butylene adipate co-terephthalate)(PBAT) copolymer using lipase B from *Candida antarctica* (CALB) and effect of PBAT on plant growth. *Polym. Bull.* **79**, 9059–9073.
37. Diaz, C.M., Gao, X., Robisson, A., Amarante, M., and Zhu, S.S. (2018). Effect of hydrolytic degradation on the mechanical property of a thermoplastic polyether ester elastomer. *Polym. Degrad. Stabil.* **155**, 35–42.
38. Held, D., and Kilz, P. (2021). Size-exclusion chromatography as a useful tool for the assessment of polymer quality and determination of macromolecular properties. *Chem. Teach. Int.* **3**, 77–103.
39. Mei, J., Dong, Z., Yi, Y., Zhang, Y., and Ying, G. (2019). A simple method for the production of low molecular weight hyaluronan by in situ degradation in fermentation broth. *E-Polymers* **19**, 477–481.
40. Reske, T., Eickner, T., Grabow, N., Schmitz, K.-P., and Siewert, S. (2020). Accelerated Degradation of polymeric surgical suture materials. *Curr. Dir. Biomed. Eng.* **6**, 458–460.
41. Chang, K.L., Tai, M.-C., and Cheng, F.-H. (2001). Kinetics and products of the degradation of chitosan by hydrogen peroxide. *J. Agric. Food Chem.* **49**, 4845–4851.
42. Andrianov, A.K., Svirkin, Y.Y., and LeGolvan, M.P. (2004). Synthesis and biologically relevant properties of polyphosphazene polyacids. *Biomacromolecules* **5**, 1999–2006.
43. Zhi, Z., Chen, J., Li, S., Wang, W., Huang, R., Liu, D., Ding, T., Linhardt, R. J., Chen, S., and Ye, X. (2017). Fast preparation of RG-I enriched ultra-low molecular weight pectin by an ultrasound accelerated Fenton process. *Sci. Rep.* **7**, 541.
44. Kucharczyk, P., Pavelková, A., Stloukal, P., and Sedlářík, V. (2016). Degradation behaviour of PLA-based polyesterurethanes under abiotic and biotic environments. *Polym. Degrad. Stabil.* **129**, 222–230.
45. Mao, S., Zhang, T., Sun, W., and Ren, X. (2012). The depolymerization of sodium alginate by oxidative degradation. *Pharm. Dev. Technol.* **17**, 763–769.
46. Launay, A., Thominette, F., and Verdu, J. (1999). Hydrolysis of poly (ethylene terephthalate): A steric exclusion chromatography study. *Polym. Degrad. Stabil.* **63**, 385–389.
47. Li, J., Nemes, P., and Guo, J. (2018). Mapping intermediate degradation products of poly (lactic-co-glycolic acid) in vitro. *J. Biomed. Mater. Res. B Appl. Biomater.* **106**, 1129–1137.
48. Otsuka, F., Pacheco, E., Perkins, L.E.L., Lane, J.P., Wang, Q., Kamberi, M., Frie, M., Wang, J., Sakakura, K., Yahagi, K., et al. (2014). Long-term safety of an everolimus-eluting bioresorbable vascular scaffold and the cobalt-chromium XIENCE V stent in a porcine coronary artery model. *Circ. Cardiovasc. Interv.* **7**, 330–342.
49. Limskon, W., Auras, R., and Selke, S. (2019). Hydrolytic degradation and lifetime prediction of poly (lactic acid) modified with a multifunctional epoxy-based chain extender. *Polym. Test.* **80**, 106108.
50. Stloukal, P., Jandikova, G., Koutny, M., and Sedlářík, V. (2016). Carbodiimide additive to control hydrolytic stability and biodegradability of PLA. *Polym. Test.* **54**, 19–28.
51. Anteunis, H., van der Meer, J.-C., de Geus, M., Kingma, W., and Koning, C.E. (2009). Improved mathematical model for the hydrolytic degradation of aliphatic polyesters. *Macromolecules* **42**, 2462–2471.
52. Kijchavengkul, T., Auras, R., Rubino, M., Alvarado, E., Camacho Montero, J.R., and Rosales, J.M. (2010). Atmospheric and soil degradation of aliphatic-aromatic polyester films. *Polym. Degrad. Stabil.* **95**, 99–107.
53. Kim, Y.-C., and McCoy, B.J. (2000). Degradation kinetics enhancement of polystyrene by peroxide addition. *Ind. Eng. Chem. Res.* **39**, 2811–2816.
54. Sterling, W.J., Kim, Y.-C., and McCoy, B.J. (2001). Peroxide enhancement of poly ( $\alpha$ -methylstyrene) thermal degradation. *Ind. Eng. Chem. Res.* **40**, 1811–1821.
55. Zhou, J., Li, L., Wang, D., Wang, L., Zhang, Y., and Feng, S. (2022). Study on Rapid Detection Method for Degradation Performance of Polyolefin-Based Degradable Plastics. *Polymers* **15**, 183.
56. Miles, C.E., Lima, M.R.N., Buevich, F., Gwin, C., Sanjeeva Murthy, N., and Kohn, J. (2021). Comprehensive hydrolytic degradation study of a new poly(ester-amide) used for total meniscus replacement. *Polym. Degrad. Stabil.* **190**, 109617.
57. Li, J., Li, S., Zheng, Y., Zhang, H., Chen, J., Yan, L., Ding, T., Linhardt, R.J., Orfila, C., Liu, D., et al. (2019). Fast preparation of rhamnogalacturonan I enriched low molecular weight pectic polysaccharide by ultrasonically accelerated metal-free Fenton reaction. *Food Hydrocoll.* **95**, 551–561.
58. McCoy, B.J., and Madras, G. (2004). Degradation kinetics of polymers in solution: Dynamics of molecular weight distributions. *AIChE J.* **43**, 802–810.
59. Wang, M., Smith, J.M., and McCoy, B.J. (1995). Continuous kinetics for thermal degradation of polymer in solution. *AIChE J.* **41**, 1521–1533.
60. McCoy, B.J., and Madras, G. (2001). Discrete and continuous models for polymerization and depolymerization. *Chem. Eng. Sci.* **56**, 2831–2836.
61. Withoeck, D., Vermeire, F., Akin, O., John Varghese, R., De Meester, S., Van Geem, K.M., and Van Steenberge, P.H.M. (2025). A novel hybrid model for pyrolysis of polystyrene using the method of moments and low molecular component balances. *Chem. Eng. J.* **505**, 159455.
62. Wu, Y.Y., Figueira, F.L., Edeleva, M., Van Steenberge, P.H.M., D'hooge, D.R., Zhou, Y.N., and Luo, Z.H. (2022). Cost-efficient modeling of distributed molar mass and topological variations in graft copolymer synthesis by upgrading the method of moments. *AIChE J.* **68**, e17559.
63. Wang, J., Wang, T.-T., Luo, Z.-H., and Zhou, Y.-N. (2023). Simulation of irreversible and reversible degradation kinetics of linear polymers using sectional moment method. *Chem. Eng. Sci.* **275**, 118711.
64. Codari, F., Lazzari, S., Soos, M., Storti, G., Morbidelli, M., and Moscatelli, D. (2012). Kinetics of the hydrolytic degradation of poly (lactic acid). *Polym. Degrad. Stabil.* **97**, 2460–2466.
65. Chen, Z., Ejiofor, E., and Peters, B. (2024). Quantifying synergy for mixed end-scission and random-scission catalysts in polymer upcycling. *React. Chem. Eng.* **9**, 139–147.
66. Ganesh, M., Dave, R.N., L'Amoreaux, W., and Gross, R.A. (2009). Embedded enzymatic biomaterial degradation. *Macromolecules* **42**, 6836–6839.

**NEWTON, Volume 1**

**Supplemental information**

**Revealing chain scission modes  
in variable polymer degradation kinetics**

**Yijie Cheng, Adolfo Lopez, Tsz Hung Wong, Darryl Francis, Emily England, and Xinyue Liu**

## **Supplemental Information**

This PDF file includes:

### **1. Supplemental Notes**

Note S1. Moment analysis for molecular weight distribution of polymers.  
Note S2. Mathematical modeling for chain-end scission.  
Note S3. Mathematical modeling for random scission.  
Note S4. Calculation of the degradable bond fraction.

### **2. Supplemental Figures**

Figure S1. Fitting polymer degradation data to chain scission modes.  
Figure S2. Time evolution of normalized molar and mass concentrations under chain-end scission.  
Figure S3. Time evolution of normalized molar and mass concentrations under random scission.  
Figure S4. Pearson correlation analysis of polymer crystallinity with chain scission preference.  
Figure S5. Chemical structures of repeat units in polylactic acid and citrus pectin.

### **3. Supplemental Tables**

Table S1. Summary of different polymer degradation with chain scission fitting and polymer characteristics.  
Table S2. Summary of different polymer degradation with chain scission fitting and polymer crystallinity.

### **4. Supplemental References**

## Supplemental Notes

### Note S1. Moment analysis for molecular weight distribution of polymers.

To describe the time evolution of molecular weight (MW) distributions during polymer degradation, we define  $P(x, t)$  as the time-dependent chain length distribution function, where  $P(x, t)dx$  represents the molar concentration of polymer chains with lengths between  $x$  and  $x + dx$  at time  $t$ . The time evolution of the chain length (that is, degree of polymerization, DOP) distribution is governed by the population balance equation, given by  $dP(x, t)/dt = F(x) - D(x)$ , where  $F(x)$  is the formation of polymer chains of length  $x$  (e.g., from scission of longer chains), and  $D(x)$  accounts for their depletion (e.g., through further cleavage). We assume that the reaction rate constant for a specific chain scission,  $k$ , is independent of chain length and time.

Solving rate expressions of chain length distributions  $dP(x, t)/dt$  leads to not only numerical solutions of the time-evolving chain length distribution  $P(x, t)$ , but also analytic solutions of averaged properties of the chain length distributions  $P^{(n)}(t)$  by using the method of moments in statistics. The moments of the chain length distributions are defined as the integrals over the chain length,  $x$ ,

$$P^{(n)}(t) = \int_0^{\infty} P(x, t) x^n dx, \quad (\text{Equation S1})$$

where the superscript  $n$  is the moment order. When  $n = 0$ , the zeroth moment  $P^{(0)}(t)$  is the total molar concentration of the *polymer*  $c_{\text{mole}}(t)$  in the unit of mol/volume. When  $n = 1$ , the first moment  $P^{(1)}(t)$  is the total molar concentration of the repeat units in the polymer in the unit of mol/volume. The product of the first moment and the molecular weight of a repeat unit,  $P^{(1)}(t) \text{ MW}_1$ , represents the mass concentration of the polymer  $c_{\text{mass}}(t)$  in the unit of mass/volume. Therefore, the number-average MW at time  $t$  is given by

$$\overline{\text{MW}(t)} = P^{(1)}(t) \text{ MW}_1 / P^{(0)}(t) = c_{\text{mass}}(t) / c_{\text{mole}}(t). \quad (\text{Equation S2})$$

At the initial time,  $t = 0$ , the number-average MW is

$$\overline{\text{MW}(0)} = P^{(1)}(0) \text{ MW}_1 / P^{(0)}(0) = c_{\text{mass}}(0) / c_{\text{mole}}(0). \quad (\text{Equation S3})$$

## Note S2. Mathematical modeling for chain-end scission.

We adopt the mathematical framework developed by McCoy et al.[S1,2] to analyze the time evolution of polymer MW distributions when subjected to chain-end scission. In this degradation mode, cleavage occurs exclusively at the terminal end of the polymer chain and generates monomers. The general chain scission reaction is expressed as



where a polymer molecule of initial chain length  $x_0$  breaks into two product molecules: a polymer fragment of length  $(x_0 - 1)$  and a monomer unit of length 1.

### 1. Population balance equations for chain length distribution

The overall chain length distribution  $P(x, t)$  under random scission follows the population balance equation  $P(x, t) = p(x, t) + q(1, t)$  and is divided into two categories below.

(i) For non-monomers ( $x > 1$ ), the population balance equation is given by

$$dp(x, t)/dt = -kp(x, t) + kp(x + 1, t), \quad (\text{Equation S5})$$

where the first term  $-kp(x, t)$  describes the depletion rate of polymer chains of length  $x$  due to cleavage, and the second term  $kp(x + 1, t)$  accounts for the formation rate of polymer chains of length  $x$  from the degradation of longer chains ( $x + 1$ ).

(ii) For the monomer products ( $x = 1$ ) which are only formed but not further degraded, the population balance equation is

$$dq(1, t)/dt = k \int_0^\infty p(x, t) dx. \quad (\text{Equation S6})$$

### 2. Moment analysis for MW evolution

To derive analytical solutions for MW evolution, we apply the moment operation  $\int_0^\infty f(x) x^n dx$  to both sides of the governing equations (Equations S5 and S6).

#### (ii) Moments for non-monomers

Applying the moment operation to Equation S5, we obtain

$$\frac{d}{dt} \int_0^\infty p(x, t) x^n dx = -k \int_0^\infty p(x, t) x^n dx + k \int_0^\infty p(x + 1, t) x^n dx. \quad (\text{Equation S7})$$

The left-hand side simplifies to

$$\frac{d}{dt} \int_0^\infty p(x, t) x^n dx = dp^{(n)}(t)/dt, \quad (\text{Equation S8})$$

where  $p^{(n)}(t)$  is the nth moment of the chain length distribution.

For the first term on the right-hand side, we obtain

$$-k \int_0^\infty p(x, t) x^n dx = -kp^{(n)}(t) \quad (\text{Equation S9})$$

For the second term on the right-hand side, we perform a variable substitution from  $x$  to  $x + 1$ , leading to

$$k \int_0^\infty p(x + 1, t) x^n dx = k \int_0^\infty p(x + 1, t) [(x + 1) - 1]^n d(x + 1). \quad (\text{Equation S10})$$

Using the binomial expansion

$$[(x + 1) - 1]^n = \sum_{j=0}^n \binom{n}{j} (-1)^{n-j} (x + 1)^j, \quad (\text{Equation S11})$$

we rewrite Equation S10 as

$$k \int_0^\infty p(x + 1, t) [(x + 1) - 1]^n d(x + 1) = k \sum_{j=0}^n \binom{n}{j} (-1)^{n-j} \int_0^\infty p(x + 1, t) (x + 1)^j d(x + 1). \quad (\text{Equation S12})$$

Since the integral form of moments is defined as  $p^{(j)}(t) = \int_0^\infty p(x, t) x^j dx$ , we simplify Equation S12 to

$$k \sum_{j=0}^n \binom{n}{j} (-1)^{n-j} \int_0^\infty p(x + 1, t) (x + 1)^j d(x + 1) = k \sum_{j=0}^n \binom{n}{j} (-1)^{n-j} p^{(j)}(t). \quad (\text{Equation S13})$$

Combining Equations S7, S8 and S13, we can derive the general rate expression for moment evolution as

$$dp^{(n)}(t)/dt = -kp^{(n)}(t) + k \sum_j \binom{n}{j} (-1)^{n-j} p^{(j)}(t). \quad (\text{Equation S14})$$

When  $n = 0$ , we evaluate the summation term in Equation S14

$$\sum_{j=0}^0 \binom{0}{j} (-1)^{0-j} p^{(j)}(t) = p^{(0)}(t). \quad (\text{Equation S15})$$

This implies

$$dp^{(0)}(t)/dt = -kp^{(n)}(t) + kp^{(n)}(t) = 0. \quad (\text{Equation S16})$$

Thus, the zeroth moment  $p^{(0)}(t)$  remains constant over time

$$p^{(0)}(t) = p^{(0)}(0). \quad (\text{Equation S17})$$

Since the initial condition of  $p^{(0)}(0)$  is equal to the initial molar concentration of polymer chains  $c_{\text{mole}}(0)$ , we obtain

$$p^{(0)}(t) = c_{\text{mole}}(0). \quad (\text{Equation S18})$$

When  $n = 1$ , we evaluate

$$\sum_{j=0}^1 \binom{1}{j} (-1)^{1-j} p^{(j)}(t) = -p^{(0)}(t) + p^{(1)}(t). \quad (\text{Equation S19})$$

Substituting this into Equation S14 gives

$$dp^{(1)}(t)/dt = -kp^{(1)}(t) + k(-p^{(0)}(t) + p^{(1)}(t)) = -kp^{(0)}(t). \quad (\text{Equation S20})$$

Since the zeroth moment is constant over time, i.e.,  $p^{(0)}(t) = p^{(0)}(0)$ , we simplify

$$dp^{(1)}(t)/dt = -kp^{(0)}(0). \quad (\text{Equation S21})$$

Thus, the first moment  $p^{(1)}(t)$  decrease linearly over time

$$p^{(1)}(t) = p^{(1)}(0) - p^{(0)}(0)kt. \quad (\text{Equation S22})$$

Since the initial condition of  $p^{(1)}(0) = c_{\text{mass}}(0)/\text{MW}_1$  and  $p^{(0)}(0) = c_{\text{mole}}(0)$ , we can obtain

$$p^{(1)}(t) = c_{\text{mass}}(0)/\text{MW}_1 - c_{\text{mole}}(0)kt. \quad (\text{Equation S23})$$

## (ii) Moments for monomer products

The above calculations consider the non-monomers with chain lengths ranging from 2 to a maximum value ( $x > 1$ ). To fully describe the system, we also need to consider the MW distribution for monomer products denoted as  $q(x, t)$  when  $x = 1$ . We notice that the right side in the monomer rate expression in Equation S6 can be rewritten in moment form as

$$k \int_0^\infty p(x, t) dx = kp^{(0)}(t). \quad (\text{Equation S24})$$

Substituting this into Equation S6, we obtain

$$dq(1, t)/dt = kp^{(0)}(t). \quad (\text{Equation S25})$$

Since the zeroth moment remains constant over time, i.e.,

$$p^{(0)}(t) = c_{\text{mole}}(0), \quad (\text{Equation S26})$$

integrating both sides of Equation S25 yields

$$q(1, t) = c_{\text{mole}}(0)kt. \quad (\text{Equation S27})$$

Since monomers consistently have a chain length of 1, their corresponding moment expressions are

$$q^{(0)}(t) = c_{\text{mole}}(0)kt, \quad (\text{Equation S28})$$

and

$$q^{(1)}(t) = c_{\text{mole}}(0)kt. \quad (\text{Equation S29})$$

## 3. Number-average molecular weight

The total molar concentration is obtained by summing the zeroth moments of both non-monomers ( $x > 1$ ) from Equation S18 and monomers from Equation S28 as

$$c_{\text{mole}}(t) = p^{(0)}(t) + q^{(0)}(t), \quad (\text{Equation S30})$$

which further gives

$$c_{\text{mole}}(t) = c_{\text{mole}}(0)(1 + kt). \quad (\text{Equation S31})$$

The total mass concentration is determined by summing the first moments of both non-monomers ( $x > 1$ ) from Equation S23 and monomers from Equation S29

$$c_{\text{mass}}(t)/\text{MW}_1 = p^{(1)}(t) + q^{(1)}(t). \quad (\text{Equation S32})$$

Multiplying the Equation S31 by  $\text{MW}_1$ , we will obtain the total mass concentration

$$c_{\text{mass}}(t) = c_{\text{mass}}(0). \quad (\text{Equation S33})$$

It indicates that the total mass is conserved throughout the degradation process. The average MW of all molecules is defined as the ratio of total mass concentration to total molar concentration, that is,

$$\overline{\text{MW}(t)} = \overline{\text{MW}(0)/(1 + kt)}. \quad (\text{Equation S34})$$

This expression provides a mathematical description of MW decay kinetics under chain-end scission. Additionally, we plot the normalized molar concentrations and normalized mass concentrations over time in **Figure S2A,B**, based on the above time-dependent expressions for both monomers and non-monomers. For the graphs in **Figure 2B-D** and **Figure S2A,B**, we assume the following values for a polydisperse polymer sample:  $c_{\text{mole}}(0) = 1 \text{ mmol L}^{-1}$ ,  $c_{\text{mass}}(0) = 5 \text{ g L}^{-1}$ ,  $\text{MW}_1 = 100 \text{ g mol}^{-1}$ .

### Note S3. Mathematical modeling for random scission.

We continue to adopt the mathematical framework developed by McCoy et al.[S1] to analyze the time evolution of MW distributions during random chain scission. Unlike chain-end scission, where cleavage occurs exclusively at the terminal bonds, random scission assumes that all backbone bonds are equally susceptible to cleavage. This results in a fragmentation process where long polymer chains randomly break into smaller fragments with varying sizes. The reaction for a polymer chain of initial length  $x_0$  undergoing random scission can be expressed as



where  $x_1$  represents the length of a newly generated polymer fragment, and  $(x_0 - x_1)$  is the remaining polymer segment. This process continues sequentially, further fragmenting the polymer chains over time, with the general reaction expressed as



where the subscript  $j$  is a serial number of degradation reactions.

#### 1. Population balance equations for chain length distribution

The overall chain length distribution  $P(x, t)$  under random scission follows the population balance equation  $P(x, t) = p(x, t) + q(x, t) + r(x, t)$  and is divided into three categories below.

(i) For undegraded reactants ( $x = x_0$ ), only depletion occurs:

$$dp(x, t)/dt = -kp(x, t). \quad (\text{Equation S37})$$

(ii) For intermediate products ( $1 < x < x_0$ ), both depletion and formation terms exist:

$$dq(x, t)/dt = -kq(x, t) + 2k \int_x^\infty \frac{q(x_i, t)}{x_i} dx_i. \quad (\text{Equation S38})$$

(iii) For final products ( $x = 1$ ), only formation occurs:

$$dr(x, t)/dt = 2k \int_x^\infty \frac{r(x_i, t)}{x_i} dx_i. \quad (\text{Equation S39})$$

#### 2. Moment analysis for MW evolution

To derive analytical solutions for MW evolution, we apply the moment operation  $\int_0^\infty f(x) x^n dx$  to both sides of the governing equations (Equations S37-39).

##### (i) Moments for undegraded reactants

For the undegraded reactants ( $x = x_0$ ), we will apply moment operation to both sides of Equation S37, yielding the moment equation

$$\frac{d}{dt} \int_0^\infty p(x, t) x^n dx = -k \int_0^\infty p(x, t) x^n dx, \quad (\text{Equation S40})$$

which simplifies to

$$dp^{(n)}(t)/dt = -kp^{(n)}(t). \quad (\text{Equation S41})$$

With the initial conditions  $p^{(0)}(0) = c_{\text{mole}}(0)$  and  $p^{(1)}(0) = c_{\text{mass}}(0)/\text{MW}_1$ , we can solve the zeroth and first moments to be

$$p^{(0)}(t) = c_{\text{mole}}(0)e^{-kt}, \quad (\text{Equation S42})$$

and

$$p^{(1)}(t) = c_{\text{mass}}(0)e^{-kt}/\text{MW}_1. \quad (\text{Equation S43})$$

##### (ii) Moments for intermediate products

For the intermediate products, the rate expression in Equation S38 for  $x_j$  can be rewritten as

$$dq(x_j, t)/dt = -kq(x_j, t) + 2k \int_{x_j}^\infty \frac{q(x_{j-1}, t)}{x_{j-1}} dx_{j-1}, \quad (\text{Equation S44})$$

where the subscript  $j$  explicitly denotes the degraded product with a specific chain length  $x_j$ . The formation term accounts for the generation of fragments with length  $x_j$ , which is from the fragmentation of a longer polymer chain of length  $x_{j-1}$  ( $x_j < x_{j-1} < x_0$ ). In this reaction, bond cleavage occurs randomly within the polymer chain  $x_{j-1}$ , meaning that each bond in  $x_{j-1}$  has an equal probability of  $1/x_{j-1}$  to break into  $x_j$ . When we apply the moment operation to both sides of Equation S44, yielding the equation for the intermediate products ( $1 < x_j < x_0$ )

$$\frac{d}{dt} \int_0^\infty q(x_j, t) x_j^n dx_j = -k \int_0^\infty q(x_j, t) x_j^n dx_j + 2k \int_0^\infty \left( \int_{x_j}^\infty \frac{q(x_{j-1}, t)}{x_{j-1}} dx_{j-1} \right) x_j^n dx_j, \quad (\text{Equation S45})$$

in which the second term on the right side can be rewritten by exchanging the integration order. Using Fubini's theorem (law for interchanging integration order in double integrals) of

$$\int_0^\infty \int_{x_j}^\infty f(x_{j-1}, x_j) dx_{j-1} dx_j = \int_0^\infty \int_0^{x_{j-1}} f(x_{j-1}, x_j) dx_j dx_{j-1}, \quad (\text{Equation S46})$$

we obtain

$$2k \int_0^\infty \left( \int_{x_j}^\infty \frac{q(x_{j-1}, t)}{dx_{j-1}} dx_{j-1} \right) x_j^n dx_j = 2k \int_0^\infty q(x_{j-1}, t) \left( \int_0^{x_{j-1}} \frac{x_j^n}{x_{j-1}} dx_j \right) dx_{j-1}. \quad (\text{Equation S47})$$

Using binomial expansion, the inner integral simplifies as

$$\int_0^{x_{j-1}} \frac{x_j^n}{x_{j-1}} dx_j = \frac{x_{j-1}^{n+1}}{n+1}, \quad (\text{Equation S48})$$

Thus, we obtain

$$2k \int_0^\infty \left( \int_{x_j}^\infty \frac{q(x_{j-1}, t)}{dx_{j-1}} dx_{j-1} \right) x_j^n dx_j = 2k \int_0^\infty q(x_{j-1}, t) \frac{x_{j-1}^n}{n+1} dx_{j-1}, \quad (\text{Equation S49})$$

which can be further rewritten as

$$2k \int_0^\infty \left( \int_{x_j}^\infty \frac{q(x_{j-1}, t)}{dx_{j-1}} dx_{j-1} \right) x_j^n dx_j = \frac{2k}{n+1} q_{j-1}^{(n)}(t). \quad (\text{Equation S50})$$

Inserting Equation S48 back to Equation S43, the differential equation of a specific intermediate product  $x_i$  is written as

$$dq_j^{(n)}(t)/dt = -kq_j^{(n)}(t) + \frac{2k}{n+1} q_{j-1}^{(n)}(t). \quad (\text{Equation S51})$$

With the initial conditions  $q_j^{(0)}(0) = q_j^{(1)}(0) = 0$ , we can solve the zeroth and first moments as

$$q_j^{(0)} = \frac{q^{(0)}(0)e^{-kt} (2kt)^{j-1}}{(j-1)!}, \quad (\text{Equation S52})$$

and

$$q_j^{(1)} = \frac{q^{(1)}(0)e^{-kt} (kt)^{j-1}}{(j-1)!}. \quad (\text{Equation S53})$$

### (iii) Moments for final products

For the final products, the rate expression in Equation S39 for  $x_j$  can be rewritten as

$$dr(x_j, t)/dt = 2k \int_{x_j}^\infty \frac{r(x_{j-1}, t)}{x_{j-1}} dx_{j-1}. \quad (\text{Equation S54})$$

where the subscript  $j$  ( $j = x_0 - 1$ ) denotes the degraded final product with a specific chain length  $x_j = 1$ . The formation term accounts for the generation of fragments with length  $x_j$ , which is from the fragmentation of a longer polymer chain of length  $x_{j-1}$  ( $x_j < x_{j-1} < x_0$ ). In this reaction, bond cleavage occurs randomly within the polymer chain  $x_{j-1}$ , meaning that each bond in  $x_{j-1}$  has an equal probability of  $1/x_{j-1}$  to break into  $x_j$ . When we apply the moment operation to both sides of Equation S54, yielding the equation for the final products ( $x_j = 1$ ), that is,

$$\frac{d}{dt} \int_0^\infty r(x_j, t) x_j^n dx_j = 2k \int_0^\infty \left( \int_{x_j}^\infty \frac{r(x_{j-1}, t)}{x_{j-1}} dx_{j-1} \right) x_j^n dx_j, \quad (\text{Equation S55})$$

Following the same steps as above, we obtain

$$dr_j^{(n)}(t)/dt = \frac{2k}{n+1} r_{j-1}^{(n)}(t), \quad (\text{Equation S56})$$

where the moment of intermediate product  $r_{j-1}^{(n)}(t)$  is equal to  $= q_{j-1}^{(n)}(t)$  provided above.

With the initial conditions  $r_j^{(0)}(0) = r_j^{(1)}(0) = 0$ , we can solve the zeroth and first moments as

$$r_j^{(0)} = p^{(0)}(0) \frac{(2k)^{j-1}}{(j-2)!} \left[ e^{-kt} \sum_{i=0}^{j-2} \frac{(-1)^{j-2-i} (j-2)! t^i}{i! (-k)^{j-1-i}} + \frac{1}{k^{j-1}} \right], \quad (\text{Equation S57})$$

and

$$r_j^{(1)} = p^{(1)}(0) \frac{k^{j-1}}{(j-2)!} \left[ e^{-kt} \sum_{i=0}^{j-2} \frac{(-1)^{j-2-i}(j-2)! t^i}{i! (-k)^{j-1-i}} + \frac{1}{k^{j-1}} \right]. \quad (\text{Equation S58})$$

The moments of both intermediate and final products can be calculated as

$$q^{(n)}(t) + r^{(n)}(t) = \sum_{j=1}^{x_0-2} q_j^{(n)}(t) + r_{x_0-1}^{(1)}. \quad (\text{Equation S59})$$

By taking the zeroth moment expressions in Equations S52 and S57 and the first moment expressions in Equations S53 and S59, we can derive the complete solution for all products ( $1 \leq x < x_0$ ). For long-chain polymers with high molecular weight ( $x_0 \rightarrow \infty$ ), the zeroth and first moments for all products can be simplified as

$$q^{(0)}(t) + r^{(0)}(t) = c_{\text{mole}}(0)(e^{kt} - e^{-kt}), \quad (\text{Equation S60})$$

and

$$q^{(1)}(t) + r^{(1)}(t) = c_{\text{mass}}(0)(1 - e^{-kt})\text{MW}_1 \quad (\text{Equation S61})$$

### 3. Number-average molecular weight

Therefore, the total molar concentration as a summation of  $p^{(0)}(t)$ ,  $q^{(0)}(t)$ ,  $r^{(0)}(t)$  is equal to

$$c_{\text{mole}}(t) = c_{\text{mole}}(0)e^{kt}. \quad (\text{Equation S62})$$

Therefore, the total mass concentration as a summation of  $p^{(1)}(t)\text{MW}_1$ ,  $q^{(1)}(t)\text{MW}_1$ ,  $r^{(1)}(t)\text{MW}_1$  is equal to

$$c_{\text{mass}}(t) = c_{\text{mass}}(0). \quad (\text{Equation S63})$$

The number-average MW is defined as the ratio of total mass concentration to total molar concentration, that is

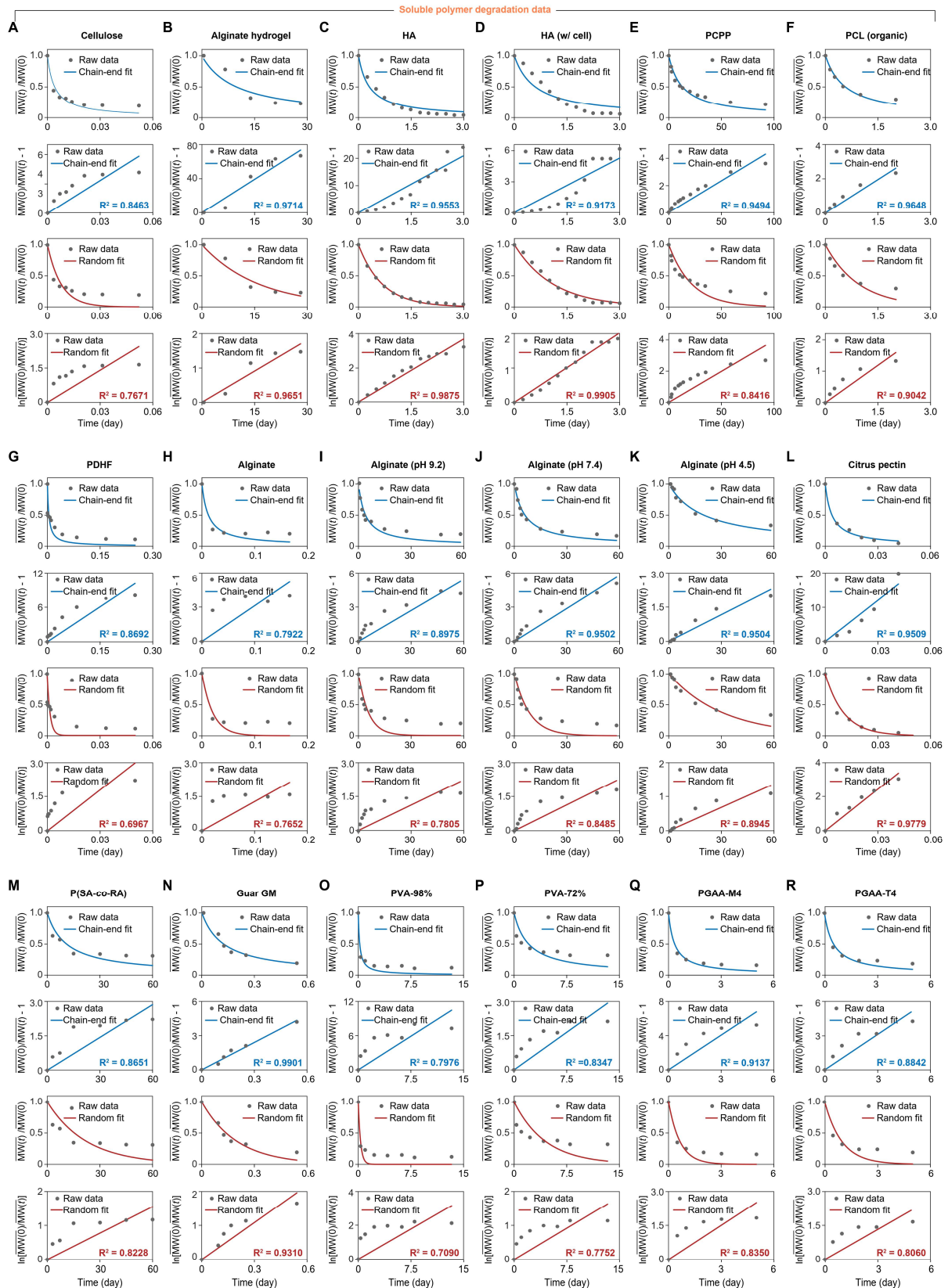
$$\overline{\text{MW}(t)} = \overline{\text{MW}(0)}e^{-kt}. \quad (\text{Equation S64})$$

This expression provides a mathematical description of MW decay kinetics under random scission. Additionally, we plot the normalized molar concentrations and normalized mass concentrations over time in **Figure S3A, B**, based on the above expressions for both undegraded reactants and degraded products. For the graphs in **Figure 2F-H** and **Figure S3A,B**, we assume the following values for a polydisperse polymer sample:  $c_{\text{mole}}(0) = 1 \text{ mmol L}^{-1}$ ,  $c_{\text{mass}}(0) = 5 \text{ g L}^{-1}$ ,  $\text{MW}_1 = 100 \text{ g mol}^{-1}$ .

**Note S4. Calculation of the degradable bond fraction.**

The fraction of degradable bonds per repeat unit is defined as the ratio of the number of degradable bonds (e.g., ester, ether, glycosidic bonds) to the total number of covalent bonds along the polymer backbone within a single repeat unit. The total bond number includes both degradable and non-degradable bonds (e.g., C–C, C–O, C–N). For PLA, the main backbone consists of three covalent bonds (i.e., two shared and two owned, calculated as  $2 \times 0.5 + 2 = 3$ , marked in blue and red). Among these, one ester bond is hydrolytically degradable (marked in red). Therefore, the fraction of degradable bonds per repeat unit in PLA is  $1/3 \approx 0.3$  (**Figure S5A**). For polymers with ring-containing repeat units (e.g., pyranose ring in alginate or aromatic ring in PET), the number of backbone bonds is determined using the shortest path principle, ensuring that only covalent bonds contributing to the continuous chain structure are counted. As illustrated in **Figure S5B**, a ring-containing repeat unit with a citrus pectin backbone is composed of ten covalent bonds (marked in blue and red), including two ether bonds (marked in red). This gives a degradable bond fraction of  $2/10 = 0.2$ . This degradable bond fraction serves as a simplified quantitative parameter to describe the intrinsic degradability of a polymer backbone, providing a consistent way to compare different polymers based on their chemical structure.

## Supplemental Figures



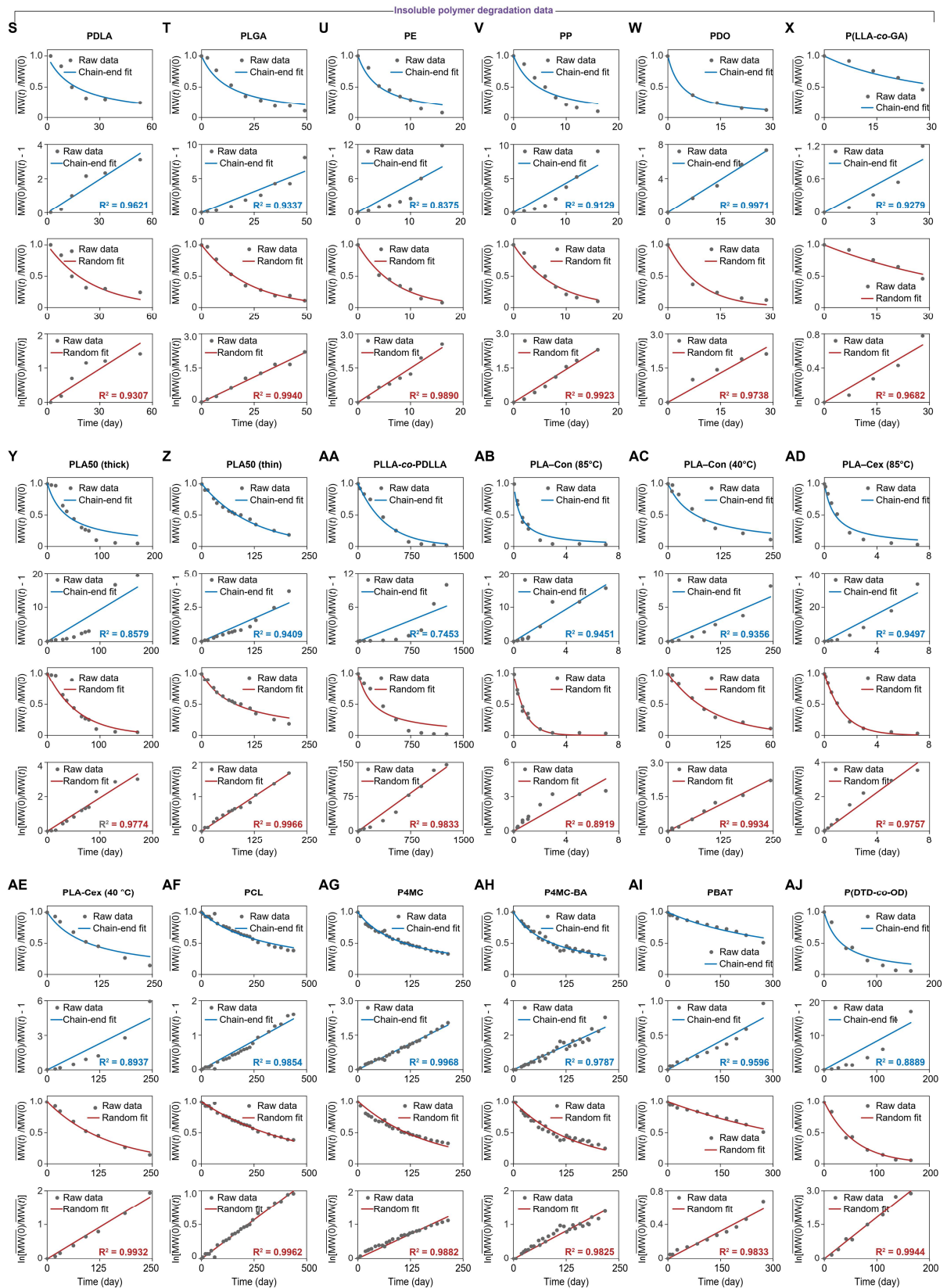


**Figure S1. Fitting polymer degradation data to chain scission modes.** The compiled data for all 41 polymers with different polymer types and degradation conditions were plotted using normalized MW decay over time. For the three selected soluble polymers (e.g., chitosan[S3], dextran[S4], PLA-co-PEG[S5]) and three insoluble polymers (e.g., PLA[S6], PLGA[S7], PET[S8]), normalized MW decay over time was plotted in **Figure 3** of the main text. The experimental data of MW decay over time for **(A)** cellulose[S9], **(B)** alginate hydrogel[S10], **(C)** hyaluronic acid (HA)[S11], **(D)** hyaluronic acid in cell culture (HA (w/cell)) [S11], **(E)** poly[di(carboxylatophenoxy)phosphazene] (PCPP)[S12], **(F)** polycaprolactone dissolved in organic solvent (PCL (organic))[S13], **(G)** poly(2,5-dihydrofuran) (PDHF)[S14], **(H)** alginate[S15], **(I)** alginate (pH 9.2)[S16], **(J)** alginate (pH 7.4)[S16], **(K)** alginate (pH 4.5)[S16], **(L)** citrus pectin[S17], **(M)** poly (sebacic acid-co-ricinoleic acid) (P(SA-co-RA))[S18], **(N)** guar galactomannan (Guar GM)[S19], **(O)** 98% hydrolyzed polyvinyl alcohol (PVA-98%)[S20], **(P)** 72% hydrolyzed polyvinyl alcohol (PVA-72%)[S20], **(Q)** poly(glycoamidoamine) with D-mannaramide (PGAA M4)[S21], **(R)** poly(glycoamidoamine) with L-tartaramide (PGAA T4)[S21], **(S)** poly(D,L-lactide) (PDLA)[S22], **(T)** poly (lactic-co-glycolic acid) (PLGA)[S7], **(U)** polyethylene (PE)[S23], **(V)** polypropylene (PP)[S23], **(W)** polydioxanone (PDO)[S24], **(X)** poly(L-lactide-co-glycolide) (P(LLA-co-GA))[S24], **(Y)** polylactic acid thick sample (PCL(thick))[S25], **(Z)** polylactic acid thin sample (PCL(thin))[S25], **(AA)** poly(L-lactide)-co-poly(D,L-lactide) (PLLA-co-PDLLA)[S26], **(AB)** neat polylactic acid at 85°C (PLA-Con (85°C))[S27], **(AC)** neat polylactic acid at 40°C (PLA-Con (40°C))[S27], **(AD)** polylactic acid with chain extender (PLA-Cex (85°C))[S27], **(AE)** polylactic acid with chain extender (PLA-Cex (85°C))[S27], **(AF)** polycaprolactone (PCL)[S28], **(AG)** poly(4-methylcaprolactone) (P4MC)[S28], **(AH)** poly(4-methylcaprolactone) with benzyl alcohol (P4MC-BA)[S28], **(AI)** polybutylene adipate-co-terephthalate (PBAT)[S29], and **(AJ)** poly(desaminotyrosyl-tyrosine dodecyl dodecanedioate) (P(DTD-co-OD))[S30] are fitted to chain-end scission (blue line) and random scission (red line) models.

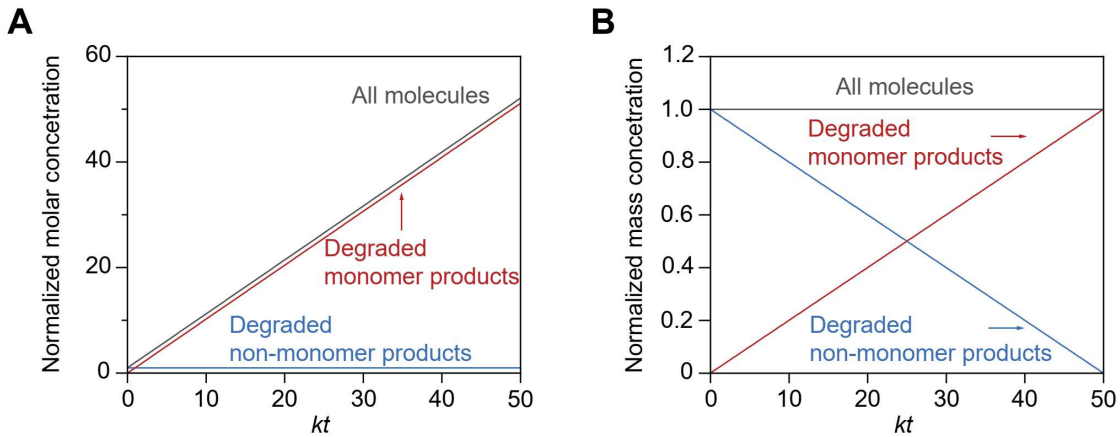


**Figure S2. Time evolution of normalized molar and mass concentrations under chain-end scission.** **(A)** Normalized molar concentrations (zeroth moments) for all molecules, degraded non-monomer products (chain length of  $x_0 - 1$ ), and degraded monomer products (chain length of 1). **(B)** Normalized mass concentrations (first moments) for all molecules, degraded non-monomer products (chain length of  $x_0 - 1$ ), and degraded monomer products (chain length of 1).

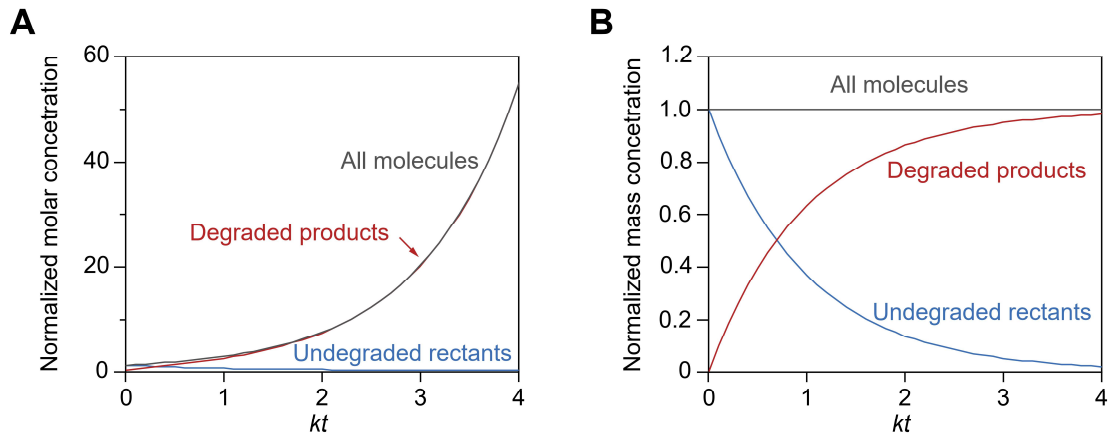


**Figure S3. Time evolution of normalized molar and mass concentrations under random scission.** **(A)** Normalized molar concentrations (zeroth moments) for all molecules, undegraded reactants (chain length =  $x_0$ ), and degraded products (chain length  $< x_0$ ). **(B)** Normalized mass concentrations (first moments) for all molecules, undegraded reactants (chain length =  $x_0$ ), and degraded products (chain length  $< x_0$ ).

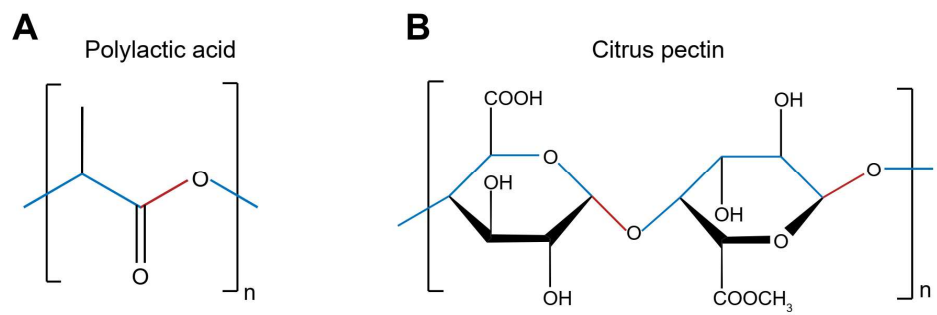


**Figure S4. Chemical structures of representative degradable polymers.** Examples: (a) polylactic acid (PLA) and (b) citrus pectin.

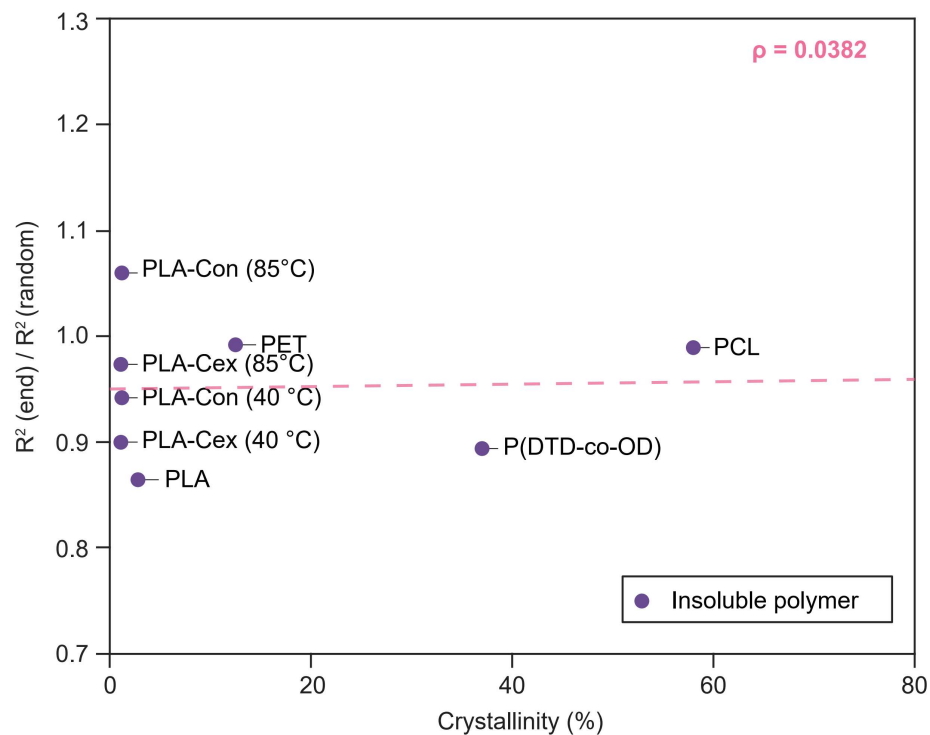


**Figure S5. Pearson correlation analysis of polymer crystallinity with chain scission preference.** The ratio of  $R^2(\text{end})$  to  $R^2(\text{random})$  is plotted against polymer crystallinity. Pearson correlation coefficient ( $\rho$ ) is indicated.

**Supplemental Tables**

**Table S1. Summary of different polymer degradation with chain scission fitting and polymer characteristics.**

No.	Polymer	Full chemical name	R <sup>2</sup> (random)	R <sup>2</sup> (end)	R <sup>2</sup> (end)/R <sup>2</sup> (chain)	Initial MW (kDa)	Deg. bond fraction	Catalyst	Catalyst size (nm)	Solubility (g per g solvent)	Deg. timescale 1/k (day)	Ref.
1	Chitosan	Chitosan	0.8818	0.9974	1.1311	213.00	0.200	Hydrogen peroxide	0.36	0.0050	0.006	S3
2	Dextran	Dextran	0.9040	0.9863	1.0910	875.30	0.200	Dextranase	6	0.0100	0.00	S4
3	PLA-co-PEG	Poly(ethylene glycol)-co-polylactide methyl ether	0.8257	0.9546	1.1561	32.64	0.333	H <sub>2</sub> O	0.28	0.0020	2.75	S5
4	Cellulose	Cellulose	0.7671	0.8463	1.1032	386.62	0.200	H <sup>+</sup> /H <sub>2</sub> O	0.28	0.0010	0.01	S9
5	Alginate hydrogel	Alginate	0.9651	0.9714	1.0065	115.66	0.200	H <sub>2</sub> O	0.28	0.0300	16.16	S10
6	HA	Hyaluronic acid	0.9875	0.9553	0.9674	1876.40	0.222	Hyaluronidase	7	0.0050	0.68	S11
7	HA (w/cell)	Hyaluronic acid	0.9905	0.9173	0.9261	1882.02	0.222	Hyaluronidase	7	0.0050	1.10	
8	PCPP	Poly[di(carboxylatophenoxy)phosphazene]	0.8416	0.9494	1.1281	820.00	1.000	H <sub>2</sub> O	0.28	0.0040	21.93	S12
9	PCL (organic)	Polycaprolactone	0.9042	0.9648	1.0670	11.67	0.143	H <sub>2</sub> O	0.28	0.0020	0.95	S13
10	PDHF	Poly(2,5-dihydrofuran)	0.6967	0.8692	1.2476	44.52	0.200	Grubbs catalysts	2	0.0052	0.01	S14
11	Alginate	Alginate	0.7652	0.7922	1.0353	345.78	0.200	Hydrogen peroxide	0.36	0.0100	0.02	S15
12	Alginate (pH 9.2)	Alginate	0.7805	0.8975	1.1499	114.35	0.200	H <sub>2</sub> O	0.28	0.0200	5.69	S16
13	Alginate (pH 7.4)	Alginate	0.8485	0.9502	1.1199	149.58	0.200	H <sub>2</sub> O	0.28	0.0200	8.61	
14	Alginate (pH 4.5)	Alginate	0.8945	0.9504	1.0625	220.71	0.200	H <sub>2</sub> O	0.28	0.0200	31.06	

No.	Polymer	Full chemical name	R <sup>2</sup> (random)	R <sup>2</sup> (end)	R <sup>2</sup> (end)/R <sup>2</sup> (chain )	Initial MW (kDa)	Deg. bond fraction	Catalyst	Catalyst size (nm)	Solubility (g per g solvent)	Deg. timescale 1/k (day)	Ref.
15	Citrus pectin	Citrus pectin	0.9779	0.9509	0.9724	451.48	0.200	Hydrogen peroxide, Fe <sup>3+</sup>	0.36	0.0050	0.01	S17
16	P(SA-co-RA)	Poly(sebacic acid-co-ricinoleic acid)	0.8228	0.8651	1.0514	3.49	0.083	H <sub>2</sub> O	0.28	0.0040	22.32	S18
17	Guar GM	Guar galactomannan	0.9310	0.9911	1.0646	1790.00	0.200	Endo-β-mannanase	3.8	0.0100	0.20	S19
18	PVA-98%	Polyvinyl alcohol, 98% hydrolyzed	0.7090	0.7976	1.1249	36.17	0.500	Microbe	6	0.0042	0.33	S20
19	PVA-72%	Polyvinyl alcohol, 72% hydrolyzed	0.7752	0.8347	1.0767	13.52	0.500	Microbe	6	0.0042	4.46	
20	PGAA-M4	Poly(glycoamidoamine) with D-mannaramide	0.8350	0.9137	1.0942	4.90	0.095	H <sub>2</sub> O	0.28	0.0245	0.97	S21
21	PGAA-T4	Poly(glycoamidoamine) with L-tartaramide	0.8060	0.8842	1.0970	5.60	0.105	H <sub>2</sub> O	0.28	0.0280	0.65	
22	PLA	Polylactic acid	0.9983	0.8630	0.8645	11.67	0.333	H <sub>2</sub> O	0.28	1E-06	7.87	S6
23	PLGA	Poly (lactic-co-glycolic acid)	0.9940	0.9337	0.9393	4.39	0.333	H <sub>2</sub> O	0.28	1E-06	22.47	S7
24	PET	Polyethylene terephthalate	0.9915	0.9834	0.9918	26.74	0.200	H <sub>2</sub> O	0.28	1E-06	13.76	S8
25	PDLA	Poly(D,L-lactide)	0.9307	0.9621	1.0337	1156.54	0.333	H <sub>2</sub> O	0.28	1E-06	25.77	S22
26	PE	Polyethylene	0.9890	0.8375	0.8468	Unknown	0.500	Microbe	10	1E-06	7.17	S23
27	PP	Polypropylene	0.9923	0.9129	0.9200	Unknown	0.500	Microbe	10	1E-06	7.67	
28	PDO	Polydioxanone	0.9738	0.9971	1.0239	Unknown	0.167	OH <sup>-</sup> /H <sub>2</sub> O	0.28	1E-06	9.06	S24
29	P(LLA-co-GA)	Poly(L-lactide-co-glycolide)	0.9687	0.9279	0.9579	Unknown	0.333	OH <sup>-</sup> /H <sub>2</sub> O	0.28	1E-06	44.44	

No.	Polymer	Full chemical name	R <sup>2</sup> (random)	R <sup>2</sup> (end)	R <sup>2</sup> (end)/R <sup>2</sup> (chain )	Initial MW (kDa)	Deg. bond fraction	Catalyst	Catalyst size (nm)	Solubility (g per g solvent)	Deg. timescale 1/k (day)	Ref.
30	PLA50 (thick)	Polylactic acid	0.9774	0.8579	0.8777	43.00	0.333	H <sub>2</sub> O	0.28	1E-06	58.02	S25
31	PLA50 (thin)	Polylactic acid	0.9966	0.9409	0.9441	67.00	0.333	H <sub>2</sub> O	0.28	1E-06	119.25	
32	PLLA-co-PDLLA	Poly(L-lactide)-co-poly(D, L-lactide)	0.9833	0.7453	0.7580	95.12	0.167	H <sub>2</sub> O	0.28	1E-06	400.00	S26
33	PLA-Con (85°C)	Polylactic acid	0.8919	0.9451	1.0596	106.10	0.333	H <sub>2</sub> O	0.28	1E-06	0.87	S27
34	PLA-Con (40°C)	Polylactic acid	0.9934	0.9356	0.9418	106.30	0.333	H <sub>2</sub> O	0.28	1E-06	105.26	
35	PLA-Cex (85°C)	Polylactic acid	0.9757	0.9497	0.9734	191.60	0.333	H <sub>2</sub> O	0.28	1E-06	1.40	
36	PLA-Cex (40°C)	Polylactic acid	0.9932	0.8937	0.8998	191.60	0.333	H <sub>2</sub> O	0.28	1E-06	147.06	
37	PCL	Polycaprolactone	0.9962	0.9854	0.9892	31.47	0.333	H <sub>2</sub> O	0.28	1E-06	434.78	S28
38	P4MC	Poly(4-methylcaprolactone)	0.9882	0.9968	1.0087	21.84	0.143	H <sub>2</sub> O	0.28	1E-06	163.93	
39	P4MC-BA	Poly(4-methylcaprolactone) with benzyl alcohol	0.9825	0.9787	0.9961	14.61	0.143	H <sub>2</sub> O	0.28	1E-06	144.93	
40	PBAT	Polybutylene adipate-co-terephthalate	0.9833	0.9596	0.9758	88.39	0.167	Microbe	20	1E-06	473.83	S29
41	P(DTD-co-OD)	Poly(desaminotyrosyl-tyrosine dodecyl dodecanedioate)	0.9944	0.8889	0.8939	59.00	0.107	H <sub>2</sub> O	0.28	1E-06	57.66	S30

**Table S2. Summary of different polymer degradation with chain scission fitting and polymer crystallinity.**

No.	Polymer	R <sup>2</sup> (end)/R <sup>2</sup> (chain)	Crystallinity (%)	Ref.
1	PLA	0.8645	59.50	S6
2	PET	0.9918	12.50	S8
3	PLA-Con (85°C)	1.0596	37.25	S27
4	PLA-Con (40°C)	0.9418	7.85	
5	PLA-Cex (85°C)	0.9734	77.70	
6	PLA-Cex (40°C)	0.8998	6.90	
7	PCL	0.9892	66.00	S28
8	P(DTD-co-OD)	0.8939	54.50	S30

### **Supplemental References**

- [S1] McCoy, B.J., and Madras, G. (2004). Degradation kinetics of polymers in solution: Dynamics of molecular weight distributions. *AIChE J.* **43**, 802-810.
- [S2] Wang, M., Smith, J., and McCoy, B.J. (1995). Continuous kinetics for thermal degradation of polymer in solution. *AIChE Journal* **41**, 1521-1533.
- [S3] Chang, K.L.B., Tai, M.-C., and Cheng, F.-H. (2001). Kinetics and products of the degradation of chitosan by hydrogen peroxide. *Journal of Agricultural and Food Chemistry* **49**, 4845-4851.
- [S4] Wang, Q., Liu, T., Xu, X., Chen, H., and Chen, S. (2021). Dextran degradation by sonoenzymolysis: Degradation rate, molecular weight, mass fraction, and degradation kinetics. *International Journal of Biological Macromolecules* **169**, 60-66.
- [S5] Kucharczyk, P., Pavelková, A., Stloukal, P., and Sedlářík, V. (2016). Degradation behaviour of PLA-based polyesterurethanes under abiotic and biotic environments. *Polymer Degradation and Stability* **129**, 222-230.
- [S6] Stloukal, P., Jandikova, G., Koutny, M., and Sedlářík, V. (2016). Carbodiimide additive to control hydrolytic stability and biodegradability of PLA. *Polymer Testing* **54**, 19-28.
- [S7] Li, J., Nemes, P., and Guo, J. (2018). Mapping intermediate degradation products of poly (lactic-co-glycolic acid) in vitro. *Journal of Biomedical Materials Research Part B: Applied Biomaterials* **106**, 1129-1137.
- [S8] Launay, A., Thominette, F., and Verdu, J. (1999). Hydrolysis of poly (ethylene terephthalate). A steric exclusion chromatography study. *Polymer degradation and stability* **63**, 385-389.
- [S9] Härdelin, L., Perzon, E., Hagström, B., Walkenström, P., and Gatenholm, P. (2013). Influence of molecular weight and rheological behavior on electrospinning cellulose nanofibers from ionic liquids. *Journal of Applied Polymer Science* **130**, 2303-2310.
- [S10] Kong, H.J., Kaigler, D., Kim, K., and Mooney, D.J. (2004). Controlling rigidity and degradation of alginate hydrogels via molecular weight distribution. *Biomacromolecules* **5**, 1720-1727.
- [S11] Mei, J., Dong, Z., Yi, Y., Zhang, Y., and Ying, G. (2019). A simple method for the production of low molecular weight hyaluronan by in situ degradation in fermentation broth. *e-Polymers* **19**, 477-481.
- [S12] Andrianov, A.K., Svirkin, Y.Y., and LeGolvan, M.P. (2004). Synthesis and biologically relevant properties of polyphosphazene polyacids. *Biomacromolecules* **5**, 1999-2006.
- [S13] Hoskins, J.N., and Grayson, S.M. (2009). Synthesis and degradation behavior of cyclic poly ( $\epsilon$ -caprolactone). *Macromolecules* **42**, 6406-6413.
- [S14] Hsu, T.-G., Liu, S., Guan, X., Yoon, S., Zhou, J., Chen, W.-Y., Gaire, S., Seylar, J., Chen, H., and Wang, Z. (2023). Mechanochemically accessing a challenging-to-synthesize depolymerizable polymer. *Nature Communications* **14**, 225.
- [S15] Mao, S., Zhang, T., Sun, W., and Ren, X. (2012). The depolymerization of sodium alginate by oxidative degradation. *Pharmaceutical development and technology* **17**, 763-769.
- [S16] Bouhadir, K.H., Lee, K.Y., Alsberg, E., Damm, K.L., Anderson, K.W., and Mooney, D.J. (2001). Degradation of partially oxidized alginate and its potential application for tissue engineering. *Biotechnology progress* **17**, 945-950.
- [S17] Zhi, Z., Chen, J., Li, S., Wang, W., Huang, R., Liu, D., Ding, T., Linhardt, R.J., Chen, S., and Ye, X. (2017). Fast preparation of RG-I enriched ultra-low molecular weight pectin by an ultrasound accelerated Fenton process. *Scientific Reports* **7**, 541.
- [S18] Ickowicz, D.E., Abtew, E., Khan, W., Golovanevski, L., Steinman, N., Weiniger, C.F., and Domb, A.J. (2016). Poly (ester-anhydride) for controlled delivery of hydrophilic drugs. *Journal of Bioactive and Compatible Polymers* **31**, 127-139.

- [S19] Tayal, A., and Khan, S.A. (2000). Degradation of a water-soluble polymer: molecular weight changes and chain scission characteristics. *Macromolecules* 33, 9488-9493.
- [S20] Solaro, R., Corti, A., and Chiellini, E. (2000). Biodegradation of poly (vinyl alcohol) with different molecular weights and degree of hydrolysis. *Polymers for Advanced Technologies* 11, 873-878.
- [S21] Liu, Y., and Reineke, T.M. (2010). Degradation of poly (glycoamidoamine) DNA delivery vehicles: polyamide hydrolysis at physiological conditions promotes DNA release. *Biomacromolecules* 11, 316-325.
- [S22] Park, T.G. (1994). Degradation of poly (D, L-lactic acid) microspheres: effect of molecular weight. *Journal of Controlled Release* 30, 161-173.
- [S23] Zhou, J., Li, L., Wang, D., Wang, L., Zhang, Y., and Feng, S. (2022). Study on Rapid Detection Method for Degradation Performance of Polyolefin-Based Degradable Plastics. *Polymers* 15, 183.
- [S24] Reske, T., Eickner, T., Grabow, N., Schmitz, K.-P., and Siewert, S. (2020). Accelerated Degradation of polymeric surgical suture materials. *Current Directions in Biomedical Engineering* 6, 458-460.
- [S25] Grizzi, I., Garreau, H., Li, S., and Vert, M. (1995). Hydrolytic degradation of devices based on poly (DL-lactic acid) size-dependence. *Biomaterials* 16, 305-311.
- [S26] Otsuka, F., Pacheco, E., Perkins, L.E., Lane, J.P., Wang, Q., Kamberi, M., Frie, M., Wang, J., Sakakura, K., and Yahagi, K. (2014). Long-term safety of an everolimus-eluting bioresorbable vascular scaffold and the cobalt-chromium XIENCE V stent in a porcine coronary artery model. *Circulation: Cardiovascular Interventions* 7, 330-342.
- [S27] Limsukon, W., Auras, R., and Selke, S. (2019). Hydrolytic degradation and lifetime prediction of poly (lactic acid) modified with a multifunctional epoxy-based chain extender. *Polymer Testing* 80, 106108.
- [S28] Antheunis, H., van der Meer, J.-C., de Geus, M., Kingma, W., and Koning, C.E. (2009). Improved mathematical model for the hydrolytic degradation of aliphatic polyesters. *Macromolecules* 42, 2462-2471.
- [S29] Kijchavengkul, T., Auras, R., Rubino, M., Alvarado, E., Montero, J.R.C., and Rosales, J.M. (2010). Atmospheric and soil degradation of aliphatic–aromatic polyester films. *Polymer Degradation and Stability* 95, 99-107.
- [S30] Miles, C.E., Lima, M.R.N., Buevich, F., Gwin, C., Sanjeeva Murthy, N., and Kohn, J. (2021). Comprehensive hydrolytic degradation study of a new poly(ester-amide) used for total meniscus replacement. *Polymer Degradation and Stability* 190, 109617.